Global Distribution of the Phase State and Mixing Times Within Secondary Organic Aerosol Particles in the Troposphere Based on Room-Temperature Viscosity Measurements

Adrian M. Maclean[1], Ying Li[2,a], Giuseppe V. Crescenzo[1], Natalie R. Smith[2], Vlassis A. Karydis[3], Alexandra P. Tsimpidi[3,4], Christopher L. Butenhoff[5], Celia L. Faiola[2,6], Jos Lelieveld[7,8], Sergey A. Nizkorodov[2], Manabu Shiraiwa[2], Allan K. Bertram[1*]

[1]Department of Chemistry, University of British Columbia, Vancouver, BC, V6T 1Z1, Canada
[2]Department of Chemistry, University of California Irvine, Irvine, CA 92697, USA
[3]Institute of Energy & Climate Research, IEK-8: Troposphere, Forschungszentrum Jülich GmbH, 52428 Jülich, Germany
[4]Institute for Environmental Research & Sustainable Development, National Observatory of Athens, 15236 Palea Penteli, Greece
[5]Dept. of Physics, Portland State University, Portland, Oregon, 97201, USA
[6]Department of Ecology and Evolutionary Biology, University of California Irvine, Irvine, CA, 92697, USA
[7]Atmospheric Chemistry Department, Max Planck Institute for Chemistry, 55128 Mainz, Germany
[8] Energy, Environment and Water Research Center, The Cyprus Institute, Nicosia 1645, Cyprus
[a] now at: Institute of Atmospheric Physics, Chinese Academy of Sciences, Beijing, 100029, China

**Correspondence to*: Allan K. Bertram (bertram@chem.ubc.ca)

Abstract

Information on the global distributions of secondary organic aerosol (SOA) phase state and mixing times within SOA is needed to predict the impact of SOA on air quality, climate, and atmospheric chemistry; nevertheless, such information is rare. In this study, we developed a parameterization for viscosity as a function of relative humidity (RH) and temperature based on room-temperature viscosity data for simulated pine tree SOA and toluene SOA. The viscosity parameterizations were then used together with tropospheric RH and temperature fields to predict SOA phase state and mixing times of water and organic molecules within SOA in the troposphere for 200 nm particles. Based on our results, the glassy state can often occur, and mixing times of water can often exceed 1 h within SOA at altitudes > 6 km. Furthermore, mixing times of organic molecules within SOA can often exceed 1 h throughout most of the free troposphere (i.e. $\gtrsim$ 1 km in altitude). In most of the planetary boundary layer (i.e. $\lesssim$ 1 km in altitude), the

glassy state is not important, and mixing times of water and organic molecules are less than 1 h. Our results are qualitatively consistent with the results from Shiraiwa et al. (Nat. Commun., 2017), although there are quantitative differences. Additional studies are needed to better understand the reasons for these differences.

TOC Graphic

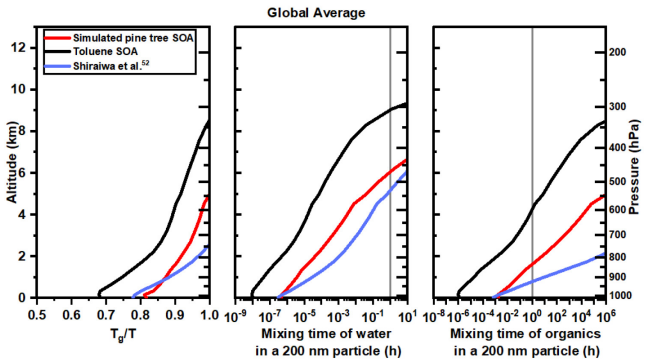

Keywords: viscosity, phase state, mixing time, secondary organic aerosol, toluene, Scots pine, free troposphere, planetary boundary layer

1 Introduction

Secondary organic aerosol (SOA) is formed in the atmosphere via gas-phase and condensed-phase reactions.[1,2] SOA can impact Earth's climate both directly, by scattering incoming solar radiation, and indirectly, by serving as nuclei for liquid cloud droplets and ice particles.[3] SOA also contributes to poor air quality, which negatively impacts visibility and heath.[4–6] It has been estimated that roughly 4.2 million deaths per year are the result of air pollution.[7,8]

Viscosity (η) is often used to specify the phase state of SOA, with $\eta < 10^2$ Pa s corresponding to a liquid, $\eta = 10^2$-10^{12} Pa s corresponding to a semisolid, and $\eta > 10^{12}$ Pa s corresponding to a glass.[9] If SOA is in a glassy state, it can act as nuclei for ice particles.[9–15] Furthermore, if the mixing time of water within a SOA particle is slow (greater than or equal to 1 h) then glassy SOA becomes more important as a nuclei for ice particles, since the slow mixing of water within SOA means a glassy SOA core can persist longer in an air parcel updraft.[16] Hence, information on the global distribution of the phase state and mixing time

of water within SOA is needed to determine when and where SOA particles can act as ice nuclei in the atmosphere.

Information on the global distribution of the mixing time of organics within SOA is also needed to predict aerosol growth, evaporation, and size distributions in chemical transport models.[17–23] If mixing times of organics within SOA are less than or equal to roughly 1 h (the time step in global chemical transport models is often 0.5 to 1 h), equilibrium partitioning of semivolatile organic compounds to the particle phase is a reasonable assumption in these models. However, if mixing times of organics are greater than roughly 1 h, non-equilibrium between semivolatile organic compounds and SOA should be considered. Slow mixing of organics within SOA can also influence reactivity within SOA.[24–34]

The phase state and mixing times of water and organic molecules within SOA particles, or proxies of SOA particles, have been investigated in many laboratory studies.[35–49] These studies have shown that the glassy state can dominate, and mixing times of water and organics are slow in SOA and SOA proxies at low temperatures and low RH values.[42,45–47] Mixing times of organic molecules within some types of SOA and SOA proxies can even exceed 1 h at room temperature if the RH is low (less than approximately 25 %).[35,44,48] However, studies assessing the global distributions of SOA phase states and mixing times within SOA are rare.

Maclean et al.[50] investigated the global distribution of mixing times of organic molecules within SOA for the planetary boundary layer (PBL), the region of the atmosphere ranging from 0 to roughly 1 km in altitude, depending on location and time.[51] To predict mixing times, a parameterization of viscosity as a function of temperature and RH was developed based on room temperature and low temperature viscosity measurements. They found that mixing times of organic molecules within SOA are commonly less than 1 h in the PBL. Shiraiwa et al.[52] investigated the global distribution of the phase state and mixing times of water and organic molecules within SOA for both the PBL and the free troposphere (FT) using a parameterization that related the glass transition temperature (T_g) to molar mass and the oxygen-to-carbon ratio (O:C) of SOA components. They found that SOA is mostly in a glassy state and mixing times of water most often exceed 1 h in the middle and upper FT, while mixing of organic molecules often exceed 1 h throughout most of the FT. Regional air quality models were also applied to simulate SOA viscosity and T_g over the U.S., finding that a glassy state is ubiquitous in the FT.[53,54]

In the following, we investigate the global distribution of the phase state and mixing times of water and organic molecules within 200 nm SOA for both the PBL and FT. We focused on SOA with diameters of 200 nm since this is a common size of SOA particles in the troposphere.[55–57] Only one study, Shiraiwa et al.,[52] previously investigated global distributions in the FT. Our approach for calculating phase state and mixing times is different from the approach taken by Shiraiwa et al.[52] In our case, we developed a parameterization for the viscosity of simulated pine tree SOA (proxy for biogenic SOA over the boreal forest) and toluene SOA (proxy for anthropogenic SOA) as a function of RH and temperature based on room-temperature viscosity measurements. This information, together with RH and temperature fields in the troposphere, was then used to estimate the global distribution of the phase state and mixing times in the PBL and FT for these types of SOA. Less parameters are required for our predictions compared to Shiraiwa et al.[52] For example, our method does not require information on the hygroscopicity or the Gordon-Taylor constants of the SOA, which have associated uncertainties leading to uncertainties in the predicted phase state and mixing times within SOA.[52] On the other hand, our method is associated with other limitations (see below), making our study complementary to the study by Shiraiwa et al.[52] We show that the glassy state and slow mixing times of water can be important at altitudes > 6 km and slow mixing of organic molecules can be important throughout most of the FT.

2 Materials and methods

To predict global distributions of SOA phase state and mixing times within SOA, we first developed parameterizations for the viscosity of simulated pine tree SOA (proxy for biogenic SOA over the boreal forest) and toluene SOA (proxy for anthropogenic SOA) as a function of RH and temperature based on laboratory viscosity measurements (Sections 2.1 and 2.2). Phase state and mixing times as a function of RH and temperature were then predicted from the RH and temperature dependent viscosities (Section 2.3). Finally, global distributions of phase state and mixing times were determined using this information and average annual RH and temperature fields in the troposphere extracted from the ECHAM/Modular Earth Submodel System Atmospheric Chemistry (EMAC) model (Section 2.5).

2.1 Parameterization for the viscosity of simulated pine tree SOA as a function of RH and temperature

We developed a parameterization for the viscosity of simulated pine tree SOA as a function of RH and temperature using the following data: 1) measured room-temperature viscosity data of SOA generated by the photooxidation of a mixture of VOCs representing emissions from healthy Scots pine (*Pinus sylvestris)* trees[58] and 2) the room temperature viscosity data of water.[59] These data are shown in Figure 1a. The measured viscosities for the simulated Scots pine tree SOA at RH values less than or equal to 50 % were taken from Smith et al.,[58] while the measured viscosities at RHs greater than 50 % are based on new measurements discussed in the supplemental information (Section S1 and S2). The measured viscosities from Smith et al.[58] were based on the poke-flow technique, and the new measurements reported in the supplemental information were based on the poke-flow technique and fluorescence recovery after photobleaching (FRAP). To determine viscosities from the poke-flow measurements, we used fluid simulations, which require material properties such as surface tension and slip length as input.[44] However, these parameters are often not well constrained for SOA material. As a result, conservative values were used in the simulations, which results in relatively large uncertainties in the viscosity data (Fig. 1a).[58] The FRAP technique involved measuring diffusion coefficients of a large fluorescent dye within the SOA material and then converting these values to viscosity using the Stokes-Einstein equation. The Stokes-Einstein equation should be able to accurately predict viscosities from measured diffusion coefficients of large organic molecules in SOA, since previous work has shown that the Stokes-Einstein equation can predict viscosities within the uncertainty of the measurements from diffusion coefficients when the radius of the diffusing molecule is similar or greater than the radius of the matrix molecules.[39]

Healthy Scots pine trees emit VOCs dominated by monoterpenes with a small contribution from sesquiterpenes.[60] A mixture of α-phellandrene, β-pinene, α-pinene, 3-carene, camphene and β-caryophyllene was used to simulate the tree emissions (see Table S1 in Smith et al.[58]). Pine trees are widely distributed throughout the boreal forest,[61] and Scots pine trees make up a significant portion of boreal forests in several European countries.[62] As a result, the simulated Scots pine tree SOA should be a good proxy for SOA over boreal forests, which represents the largest biome by area on Earth. The applicability of these results to other types of biogenic SOA still needs to be determined. Simulated pine

tree SOA was used as proxy for biogenic SOA for this study in the place of the more frequently used α-pinene SOA. Previous studies have found differences between SOA generated from multiple VOC precursors versus the simpler model systems often used (α-pinene SOA).[63–66]

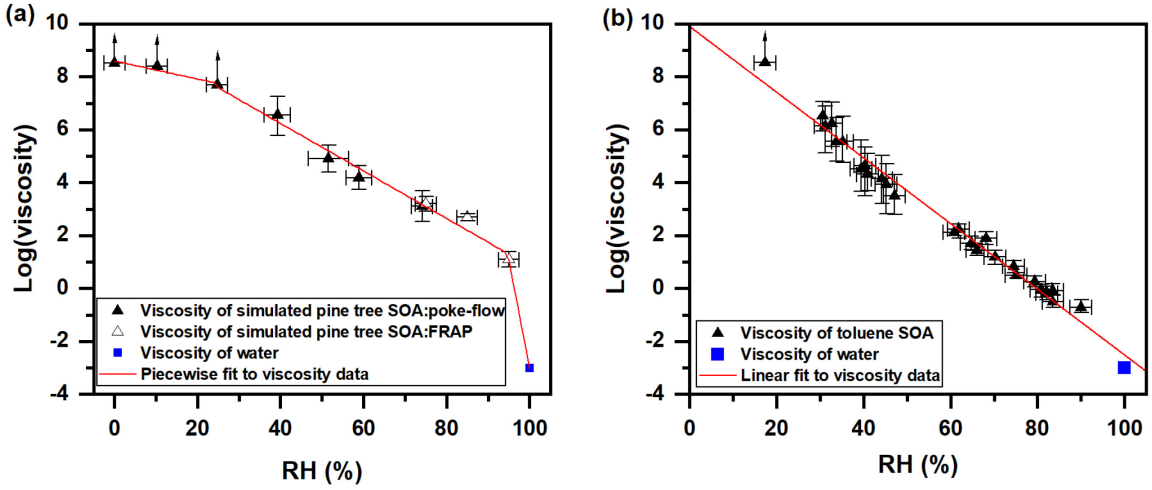

Figure 1. Panel a shows the log(viscosity) data from Smith et al.[58] as a function of the activity of water (RHs < 50%) and new measurements (RHs > 50%) using poke-flow and fluorescence recovery after photobleaching (FRAP) (Section S1 and S2) for simulated pine tree SOA, the viscosity of pure water, as well as a fit to the data using eq 1-3. Panel b shows the log(viscosity) data from Song et al.[48] as a function of the activity of water for toluene SOA, the viscosity of pure water, and a fit to the data using eq 6. For both panels the x-error bars represent uncertainties in the RH measurements and the y-error bars correspond to the upper and lower limits of the viscosities. The points with upwards arrows correspond to data where only lower limits of viscosity were obtained.

To generate a parameterization for viscosity as a function of RH and temperature, we first fit the data in Figure 1a piecewise to the following equations:

$$\log(\eta(RH, 294K)) = \begin{cases} \left(1 - \frac{RH}{100}\right) a + \frac{RH}{100} b, & RH \leq 24.75\ \%, (1) \\ \left(1 - \frac{RH}{100}\right) c + \frac{RH}{100} d, & 24.75 < RH < 95\ \%, (2) \\ \left(1 - \frac{RH}{100}\right) e + \frac{RH}{100} f, & RH \geq 95\ \%, (3) \end{cases}$$

where $\eta(RH, 294K)$ is the RH-dependent viscosity at 294 K (i.e. room temperature) and a-f are fitting parameters. The values for coefficients [*a, b, c, d, e, f*] were [8.60 ± 0.16, 5.19 ± 0.90, 9.83 ± 0.33, 0.85

± 0.21, 78.89, -3.02], respectively, based on the fitting. The results from the fitting are shown in Figure 1a (solid line). These equations were used since they monotonically decrease as the RH increases and since they fit the data well for their respective RH ranges. Equations 1-3 are equivalent to an activity-based viscosity mixing rule (see Supplement, Section S3) used previously with some success to predict viscosity in organic-water mixtures.[42]

To extrapolate the room-temperature viscosity data, η(RH, 294K), to other temperatures we used the Vogel-Tammann-Fulcher (VTF) equation:

$$\eta(RH,T) = \eta_\infty e^{\frac{T_0(\mathrm{RH})D_\mathrm{f}}{T-T_0(\mathrm{RH})}}, \quad (4)$$

where η(RH,T) is the RH and temperature dependent viscosity, η_∞ is the viscosity at infinite temperature (10^{-5} Pa s based on Angell),[67,68] D_f is the fragility parameter, and T_0(RH) is the RH dependent Vogel temperature. This is the same equation used by Shiraiwa et al.[52] to calculate viscosities as a function of temperature from T_g. We first calculated T_0(RH) from the room-temperature viscosity parameterization discussed above by rearranging the VTF equation and evaluating at T = 294 K:

$$T_0(RH) = \frac{\ln\left(\frac{\eta(\mathrm{RH},294\ \mathrm{K})}{\eta_\infty}\right)294\ K}{D_\mathrm{f}+\ln\left(\frac{\eta(\mathrm{RH},294\mathrm{K})}{\eta_\infty}\right)}, \quad (5)$$

To be consistent with Shiraiwa et al.,[52] we assumed D_f = 10. The fragility parameter for organic compounds are typically in the range of ~5-30.[69] Furthermore, for molar masses greater than 200 g mol^{-1}, D_f is typically in the range of 5-20 and approaches a limit of ~10 at molar masses greater than 400 g mol^{-1}.[70] The value of D_f was assumed to be independent of RH.[52,70–72] This assumption was consistent with previous studies that found that the value of D_f in sucrose and citric acid were independent of water content, except when the water content was very low.[68,73,74] After T_0(RH) was calculated, we calculated η(RH,T) using eq 4.

2.2 Parameterization for the viscosity of toluene SOA as a function of RH and temperature

We developed a parameterization for the viscosity of toluene SOA (proxy of anthropogenic SOA) as a function of RH and temperature using the following data: 1) measured room-temperature viscosity data of SOA generated via the photooxidation of toluene[48] and 2) the room temperature viscosity data of water.[59] These data are shown in Figure 1b. Aromatic hydrocarbons (including toluene) are an important

source of SOA in urban environments,[75,76] and toluene SOA is often used as a proxy for anthropogenic SOA.[77,78] Furthermore, the RH-dependent viscosity of toluene SOA is similar to the RH-dependent viscosity of SOA generated from diesel fuel vapors.[79] Diesel fuel vapors contain a mixture of volatile organic compounds, and SOA generated from these vapors is likely a good proxy for SOA from anthropogenic sources.[75,80–83]

To generate a parameterization for viscosity of toluene SOA as a function of RH and temperature, we first fit the data in Figure 1b to an activity-based viscosity mixing rule (eq 6):

$$\log(\eta(RH, 294K)) = (1 - \frac{RH}{100})g + \frac{RH}{100}h, \quad (6)$$

The value of coefficients [*g, h*] were [9.89 ± 0.20, -2.52 ± 0.15], respectively, based on the fitting. The results of the fitting are included in Figure 1b (solid line). Equation 6 was used to fit the data since the logarithm of viscosity monotonically decreases as the RH increases and it fit the data well. To extrapolate the room-temperature viscosity data, η(RH, 294K), to other temperatures, we used the same approach discussed above for simulated pine tree SOA.

2.3 Predicting phase state and mixing times

To determine if the SOA was in a glassy state, we first calculated the glass transition temperature of the SOA as a function of RH using the following equation:

$$T_g(RH) = \frac{T_o(RH) * (D_f + 39.17)}{39.17}, \quad (7)$$

where T_g(RH) is the RH dependent glass transition temperature of the SOA. Equation 7 was derived using the VTF equation (eq 4) and assuming $\eta = 10^{12}$ Pa s at the glass transition temperature.[67,68,70] Next, the variable T_g(RH)/T was evaluated, and a T_g(RH)/T value ≥ 1 was assumed to correspond to the glassy state.

To determine mixing times of organic molecules within SOA, we first calculated diffusion coefficients of organic molecules within SOA as a function of temperature and RH from η(RH,T) using the Stokes-Einstein equation:

$$D_{org}(RH, T) = \frac{kT}{6\pi\eta_{org}(RH,T)R_{diff}}, \quad (8)$$

where D_{org}(RH,T) is the RH and temperature dependent diffusion coefficient of organic molecules within SOA, k is the Boltzmann constant, and R_{diff} is the radius of the diffusing molecules. Although the Stokes-Einstein equation drastically underpredicts diffusion coefficients of water and small oxidants in organic-water mixtures, it predicts diffusion coefficients within the uncertainty of the measurements for the majority of the cases reported in the literature when the radius of the diffusing molecule (R_{diff}) is greater than or equal to the radius of the matrix molecules (R_{matrix}).[39] The value of R_{matrix} represents the average radius of the organic molecules that make up the SOA particles, whereas R_{diff} represents the radius of the molecules of interest diffusing through the SOA. For the case of organic diffusion, we assumed R_{diff} = R_{matrix}, meaning that the radius of the diffusing molecules was the same size as the average radius of the SOA molecules. For our calculations, we used a R_{diff} value of 0.4 nm, which was consistent with molecular weights, densities, and an assumed spherical geometry of SOA molecules.[44,58,84–91] In contrast, Shiraiwa et al.[52] used a value of 0.1 nm for the radius of the diffusing organic molecules. This results in a difference of only a factor of 4 in the mixing times of organic molecules according to eq 8, which is small compared to the variability in the mixing times considered here (greater than 5 orders of magnitude in variability). Nevertheless, when comparing our results with Shiraiwa et al.[52], all of the organic mixing times from Shiraiwa et al.[52] were increased by a factor of 4 to be consistent with the radius of the diffusing molecules used in our study.

After determining D_{org}(RH,T), we calculated mixing times of organic molecules as a function of RH and temperature, $\tau_{mix,org}$(RH,T), using the following equation:[92]

$$\tau_{\mathrm{mix,org}}(RH,T) = \frac{d_p^2}{4\pi^2 D_{\mathrm{org}}(RH,T)}, \quad (9)$$

where d_p is the diameter of the SOA particle. The diameter of the SOA particle was assumed to be 200 nm, as that is a common size of SOA particles in the atmosphere.[55–57] This mixing time corresponds to the time it takes for concentration of the diffusing species at the centre of the particle to reach ~37% (1/e) of the equilibrium concentration.

To determine mixing times of water within SOA, diffusion coefficients of water as a function of RH and temperature were determined using the fractional Stokes-Einstein equation:[38,39,93]

$$D_{\mathrm{H2O}}(RH,T) = D_0(\mathrm{T}) * \left(\frac{\eta_0(\mathrm{T})}{\eta(\mathrm{RH,T})}\right)^{\xi}, \quad (10)$$

where D_{H2O} (RH, T) is the RH and temperature dependent diffusion coefficient of water in SOA, D_0(T) is the temperature dependent diffusion coefficient of water in pure water, ξ is the fractional exponent, and η_0(T) is the temperature-dependent viscosity of pure water. The temperature-dependent viscosity data for pure water were taken from Hallett[94] and Crittenden et al.[59] Details can be found in Section S4. D_0(T) was evaluated using the Stokes-Einstein equation and assuming a radius for a molecule of water of 0.1 nm.[93] The value of the fractional exponent was calculated using eq 11:[38]

$$\xi = 1 - \left[Aexp\left(-B\frac{R_{diff}}{R_{matrix}}\right)\right], \quad (11)$$

where A and B are coefficients with values of 0.73 and 1.79, respectively. To evaluate eq 11, we assumed R_{diff} = 0.1 nm and R_{matrix} = 0.4 nm to be consistent with the size of water and organic molecules, respectively, as discussed above. The fractional Stokes-Einstein equation (eq 10) combined with eq 11 was able to predict 98 % of the published diffusion coefficients of small molecules, including water, within the uncertainties of the measurements for organic-water mixtures.[38] Once D_{H2O} (RH, T) was determined using eq 10 and 11, we then calculated mixing times of water within the SOA using an equation similar to eq 9. To calculate diffusion coefficients of water, we used the fractional Stokes-Einstein equation in place of the method used by Shiraiwa et al.[52] because the fraction Stokes-Einstein equation does not require any assumption about the hygroscopicity or density of the SOA , unlike the method used by Shiraiwa et al.[52]

2.4 Predicting phase state and mixing times from Shiraiwa et al.[52]

Shiraiwa et al.[52] used the EMAC atmospheric chemistry-climate model which includes the organic aerosol module ORACLE to simulate the mass of biogenic and anthropogenic SOA in four separate volatility bins.[95,96] Each volatility bin was then assigned molar masses and oxygen-to-carbon ratios (O:C) based on the molecular corridor approach.[97] The glass transition temperature (T_g) for each bin was then calculated from the molar mass and O:C using a parameterization developed by Shiraiwa et al.[52] The glass transition temperature as a function of RH of the total SOA (biogenic and anthropogenic SOA combined) was then calculated from the glass transition temperature of each volatility bin and the Gordon-Taylor approach. Viscosities and mixing times were then calculated as a function of temperature and RH from the RH dependent glass transition temperature of the total SOA. One consequence of this approach was their

predictions corresponded to the total SOA (biogenic and anthropogenic SOA), rather than biogenic and anthropogenic SOA separately, although it should be kept in mind that on a global scale biogenic SOA dominates over anthropogenic SOA. Shiraiwa et al.[52] mostly focused on results from three atmospheric pressures: surface pressure, 850 hPa, and 500 hPa. Here, for comparison purposes, the predictions from Shiraiwa et al.[52] are replotted as a function of latitude and altitude. As mentioned above, their mixing times for organic molecules within SOA were increased by a factor of 4 to be consistent with the radius of the organic diffusing molecule used in our study.

2.5 RH and temperature in the troposphere

Information on the RH and temperature in the troposphere is needed to assess the phase of the SOA and the mixing times within the particles. Average annual RH and temperature fields were calculated using the model EMAC for the years 2005-2009. The same RH and temperature fields were used by Shiraiwa et al.[52] RH and temperature were determined as functions of pressure, latitude, and longitude. From the pressure, the altitude (h) was calculated using eq 12:[98]

$$h = \frac{1-(\frac{P}{P_0})^{\frac{R\lambda}{gM_{\text{air}}}}}{\frac{\lambda}{T_0}}, \quad (12)$$

where P_0 is the pressure at sea level (101325 Pa), P is the pressure at the altitude being calculated, R is the gas constant (8.3145 J mol^{-1} K^{-1}), λ is the temperature lapse rate (6.5 K km^{-1}), g is the standard gravity (9.806 m s^{-2}), M_{air} is the molecular mass of air (28.97 g mol^{-1}), and T_0 is the temperature at the surface (288.15 K). Temperature and RH values were averaged across longitude to give values as a function of latitude and altitude (Figure 2).

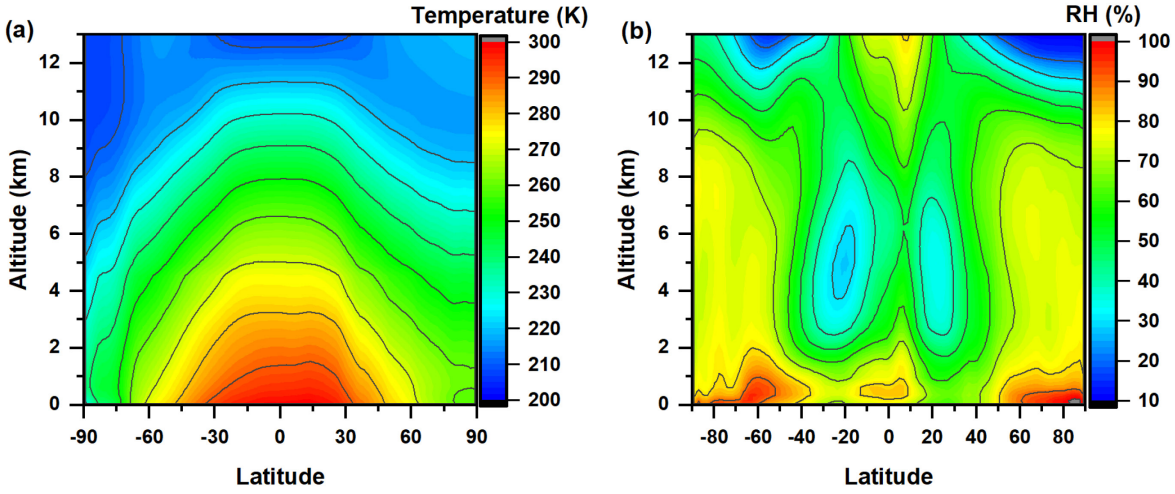

Figure 2. Altitude profiles for a) temperature and b) relative humidity (RH) as a function of latitude calculated using the EMAC model for the years 2005-2009.

3 Results and discussion

3.1 Parameterization of the viscosity, T_g/T, and mixing times of SOA particles as a function of temperature and RH.

Shown in Figure 3 are the parameterizations of viscosity, T_g/T, and mixing times as a function of RH and temperature developed using the procedures described above. Here we highlight a few points: 1) as expected, the viscosity depends strongly on RH and temperature, with the viscosity increasing as the RH and temperature decrease (Figure 3a-b). An increase in viscosity with a decrease in RH is expected since water is a plasticizer and a decrease in RH leads to a decrease in the water content of the SOA. An increase in viscosity with a decrease in temperature is expected since viscous flow is an activated process. 2) At RH = 0, the simulated pine tree SOA and toluene SOA are in a glassy state at temperatures $\leq$ 280 K and $\leq$ 285 K, respectively (Figure 3 c-d). This illustrates that SOA can be in a glassy state at temperatures approaching room temperature if RH is very low, though such conditions are not commonly expected in the atmosphere. However, it should be kept in mind that the glass transition temperature is highly dependent on RH. For example, at RH = 60%, the simulated pine tree SOA and toluene SOA do not reach the glassy state until the temperature is $\leq$ 250 K and $\leq$ 235 K, respectively. 3) At the same RH and

temperature, the mixing times of organics are much longer than the mixing times of water within the same type of SOA. For example, at 0% RH and 280 K, the mixing times of organics are at least a factor of 10^8 larger than the mixing times of water within the simulated pine tree SOA (Figure 3e & 3g). This is because small molecules, such as water, can more easily diffuse through SOA particles than larger organic molecules.

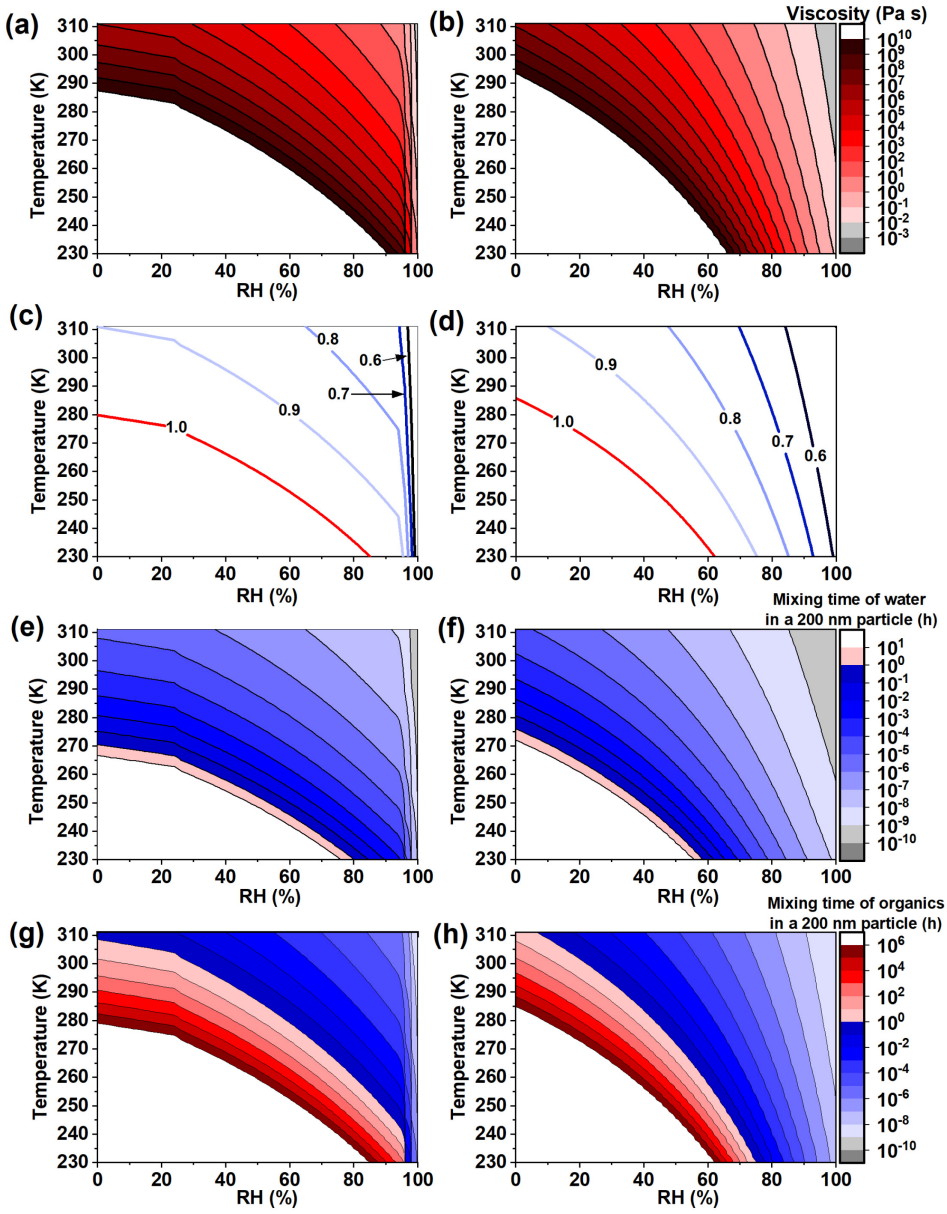

Figure 3. Properties of simulated pine tree SOA and toluene SOA as a function of temperature and RH. Panels (a, b) correspond to viscosity for a) simulated pine tree SOA and b) toluene SOA as a function of temperature and RH. Panels (c, d) correspond to T_g/T for c) simulated pine tree SOA and d) toluene SOA as a function of temperature and RH. Mixing times of water in a 200 nm particle are shown in panels (e, f) for e) simulated pine tree SOA and f) toluene SOA. Mixing times of organic molecules in a 200 nm particle are shown in panels (g, h) for g) simulated pine tree SOA and h) toluene SOA.

3.2 Global distributions of the glassy state

Shown in Figure 4 are predicted annual average T_g/T values as a function of altitude and latitude for simulated pine tree SOA (Figure 4a) and toluene SOA (Figure 4b). As mentioned above, SOA is in a glassy phase state when $T_g/T \geq 1$. The altitude above which SOA was expected to vitrify was in the FT region and depended on the latitude. To better illustrate the latitudinal dependence, Figure 5 shows the annual average T_g/T values as a function of altitude for the tropical regions (-23.26° to 23.26°), midlatitude regions (-23.26° to -66.3° and 23.26° to 66.3°), and polar regions (less than -66.3° and greater than 66.3°). The patterns of T_g/T as a function of altitude and latitude were similar in the northern and southern hemisphere (Figure 4) since the patterns of RH and temperature as a function of altitude and latitude were similar in both hemispheres (Figure 2). In addition, the shape of the $T_g/T = 1$ isopleth for simulated pine tree SOA was similar to toluene SOA, except the $T_g/T = 1$ isopleth for toluene SOA occurred at 1-2 km higher in altitude. Based on Figure 4, the lowest altitude at which the glassy state was observed was 0 km for simulated pine tree SOA and 5 km for toluene SOA, occurring at a latitude of -90° and -30°, respectively. The glassy state should be rare in the PBL, based on these predictions.

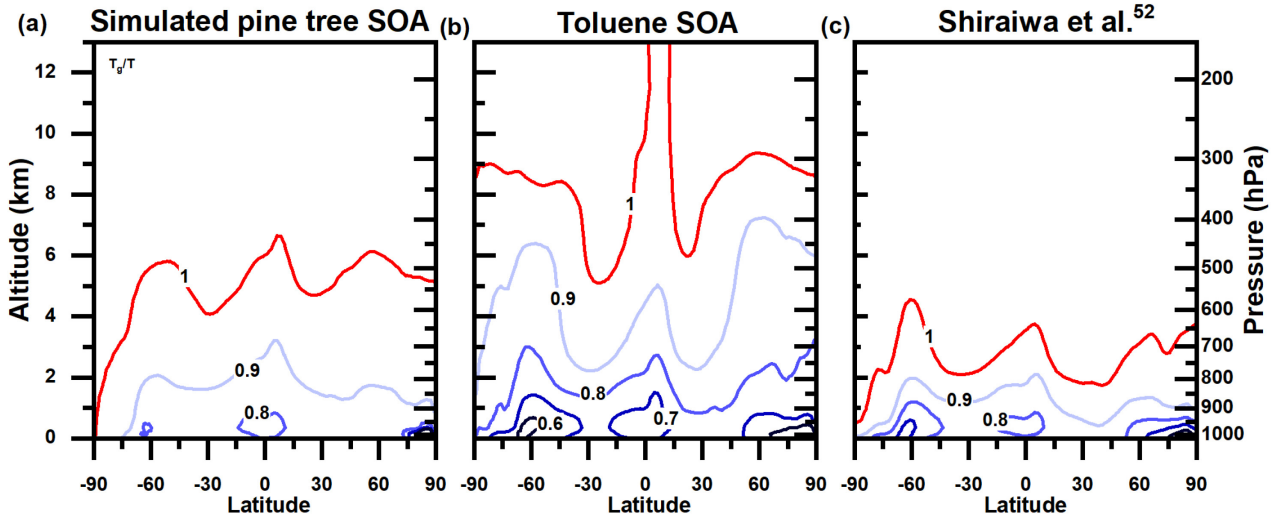

Figure 4. Annual average phase state of particles of a) simulated pine tree SOA, b) toluene SOA, and c) SOA from Shiraiwa et al.[52] as a function of altitude and latitude. The particles are in the glassy state when $T_g/T \geq 1$. The red contour line corresponds to T_g/T=1.

The glassy phase state first occurs at a latitude of -90° but not 90° for the simulated pine tree SOA due to the difference in temperatures. At a latitude of -90°, the temperature was ~30 K lower than the temperature at 90°, resulting in higher viscosities.

For simulated pine tree SOA in the polar, midlatitude, and tropical regions, the annual average T_g/T could exceed 1, indicating the formation of a glass, at altitudes of 4.25 km, 5.25 km, and 5.5 km, respectively (Figure 5a). For toluene SOA in the polar, midlatitude, and tropical regions, the average T_g/T could exceed 1 at altitudes of 8.75 km, 8.5 km, and 7.25 km, respectively (Figure 5b).

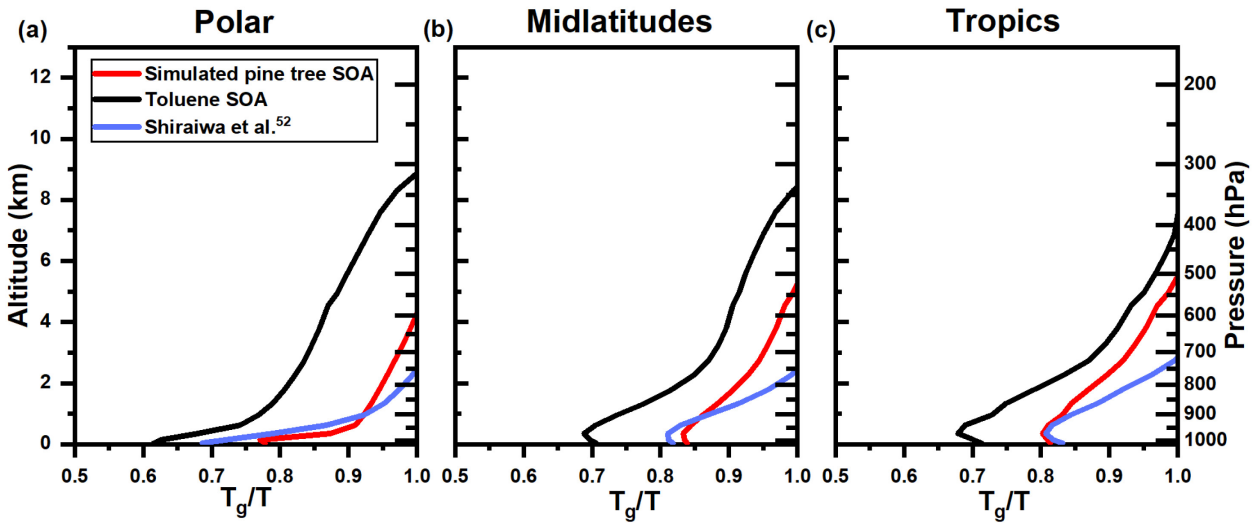

Figure 5. Annual average altitude profiles of T_g/T for a) polar (latitude greater than 66.3° and less than -66.3°), b) midlatitude (66.3°>latitude>23.26° and -66.3°<latitude<-23.26°), and c) tropical (23.26°>latitude>-23.26°) regions for simulated pine tree SOA (red), toluene SOA (black), and SOA from Shiraiwa et al.[52] (blue).

The results from Shiraiwa et al.[52] are shown in Figures 4c and 5 for comparison. As discussed above, their results corresponded to combined biogenic and anthropogenic SOA. However, biogenic sources dominate outside urban environments and in the FT since anthropogenic sources only contribute approximately 10% to the total SOA budget.[2,99] The predictions from Shiraiwa et al.[52] had a similar shape to the results for simulated pine tree SOA and toluene SOA (Figure 4c), except the $T_g/T = 1$ isopleth was shifted to lower altitudes. The T_g/T=1 isopleth from Shiraiwa et al.[52] was approximately 1-4 km lower in attitude than the simulated pine tree SOA predictions, depending on latitude. At a latitude of -90°, the lowest altitude at which the glassy state might be observed is 0.5 km based on the results from Shiraiwa et al.[52]

For the polar, midlatitude, and tropical regions the average T_g/T might exceed 1 at altitudes of 2.5 km, 2.5 km, and 3 km, respectively, based on Shiraiwa et al.[52] The glassy state was also rare in the PBL except over dry lands based on the Shiraiwa et al.[52] predictions.

3.3 Global distributions of water mixing times

Shown in Figures 6-7 are the predicted global distributions of the annual average mixing times of water in 200 nm particles. The shapes of the 1 h isopleth for simulated pine tree SOA were similar to the 1 h isopleth for toluene SOA, except the toluene SOA 1 h isopleth occurred at 2-3 km higher in altitude. Based on Figure 6, the lowest altitude where the mixing times of water were greater than or equal to 1 h was 1.5 km for simulated pine tree SOA and 8 km for toluene SOA, occurring at latitudes of -90° and -30°, respectively. The mixing time of water reaching 1 h for the simulated pine tree SOA at a latitude of -90°, but not 90°, due to the lower temperatures at -90° compared to 90°, as discussed above. For simulated pine tree SOA in the polar, midlatitude, and tropical regions, the average mixing time of water was greater than or equal to 1 h at altitudes of 5 km, 6.5 km, and 6.75 km, respectively (Figure 7a). For toluene SOA in the polar, midlatitude, and tropical regions, the average mixing time of water was greater than or equal to 1 h at altitudes of 9 km, 8.75 km, and 9.5 km, respectively (Figure 7b).

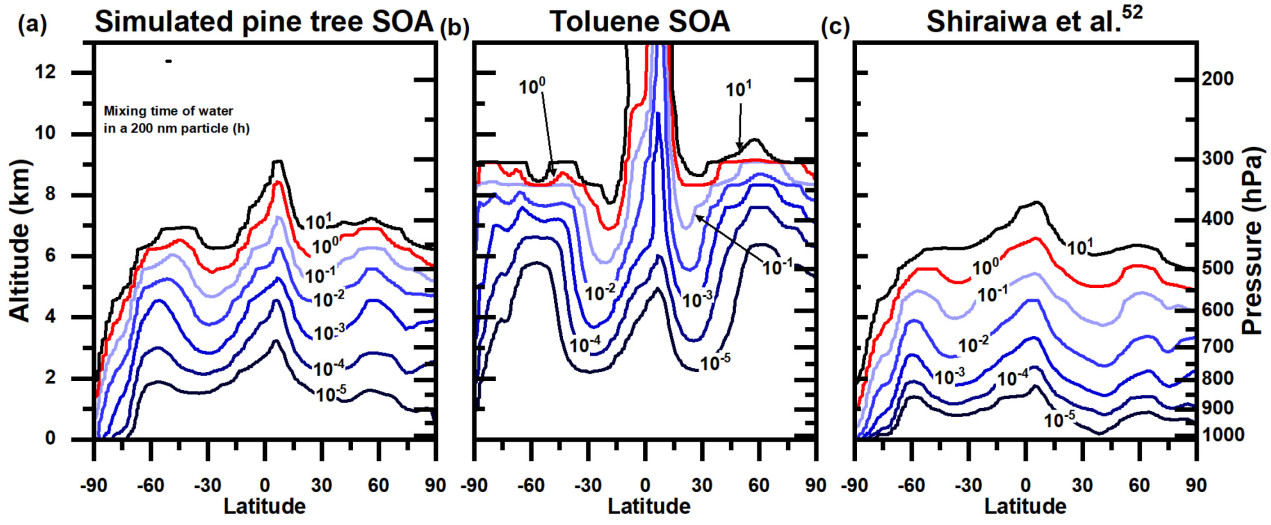

Figure 6. Annual average mixing time of water in a 200 nm particle for a) simulated pine tree SOA, b) toluene SOA, and c) SOA from Shiraiwa et al.[52] as a function of altitude and latitude. The contour lines correspond to mixing times in hours. The red contour line corresponds to a mixing time of 1 h.

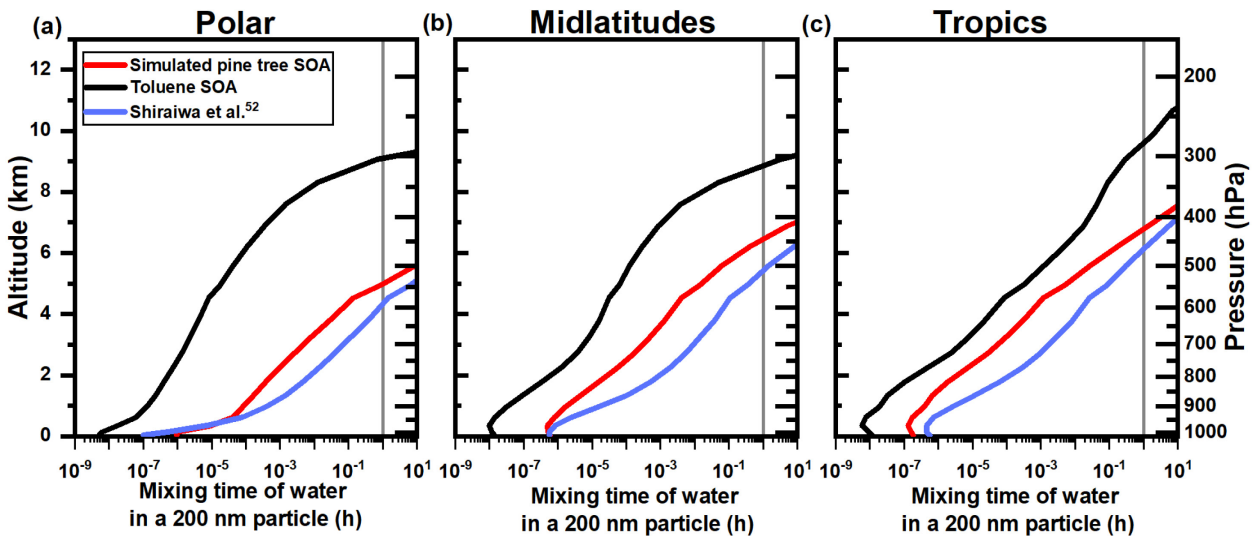

Figure 7. Annual average altitude profiles of the mixing time of water in a 200 nm particle for a) polar (latitude greater than 66.3° and less than -66.3°), b) midlatitude (66.3°>latitude>23.26° and -66.3°<latitude<-23.26°), and c) tropical (23.26°>latitude>-23.26°) regions for simulated pine tree SOA (red) , toluene SOA (black), and SOA from Shiraiwa et al.[52] (blue). The vertical lines are included to highlight a mixing time of 1 h. Average mixing time values were calculated using the average of the log mixing time data as a function of latitude.

The results from Shiraiwa et al.[52] had a similar shape to the simulated pine tree SOA and toluene SOA results (Figure 6c), except that the 1 h isopleth was at lower altitudes. At a latitude of -90° (Figure 6c), Shiraiwa et al.[52] predicted the mixing time of water to be greater than 1 h at altitudes of 1 km. The average mixing time of water in polar, midlatitude, and tropical regions could be greater than 1 h at altitudes of 4.5 km, 5.5 km, and 6 km, respectively (Figure 7).

3.4 Global distributions of organic mixing times

Shown in Figures 8-9 are the predicted global distributions of annual average mixing times of organic molecules in 200 nm particles. The lowest altitude at which the mixing times of organics exceeded 1 h was 0 km for simulated pine tree SOA (Figure 8a) and 1.5 km for toluene SOA (Figure 8b), corresponding to -90° latitude. The mixing times of organics were less than 1 h in the PBL based on both the simulated pine tree and toluene SOA predictions.

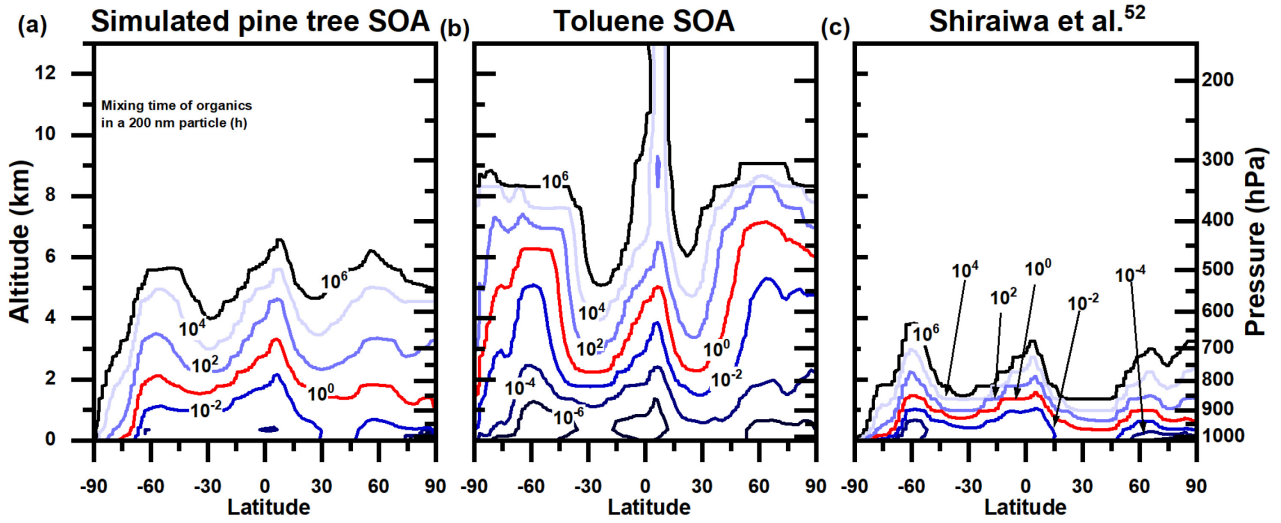

Figure 8. Annual average mixing time of organic molecules within SOA for a) simulated pine tree SOA, b) toluene SOA, and c) SOA from Shiraiwa et al.[52] as a function of altitude and latitude. The contour lines correspond to mixing times in hours. The red contour line corresponds to a mixing time of 1 h.

Simulated pine tree SOA in the polar, midlatitude, and tropical regions could have an average mixing time of organics ≥ 1 h at altitudes of 0.5 km, 1.75 km, and 2.5 km, respectively (Figure 9). Toluene SOA in the polar, midlatitude, and tropical regions could have an average organic mixing time ≥ 1 h at altitudes of 5.75 km, 4 km, and 3.5 km, respectively (Figure 9).

Similarly to T_g/T and the water mixing times, the results for the mixing time of organics by Shiraiwa et al.[52] had a similar shape to the simulated pine tree and toluene SOA results (Figure 8c), except the 1 h isopleth occurred at a lower altitude. At a latitude of -90° (Figure 8c), the mixing time of organics could exceed 1 h at the surface. The average mixing times of organics in the polar, midlatitude, and tropical regions could be greater than 1 h at altitudes of 0.5 km, 1 km, and 1 km, respectively (Figure 9). The mixing times of organics were often less than 1 h in the PBL based on the Shiraiwa et al.[52] predictions.

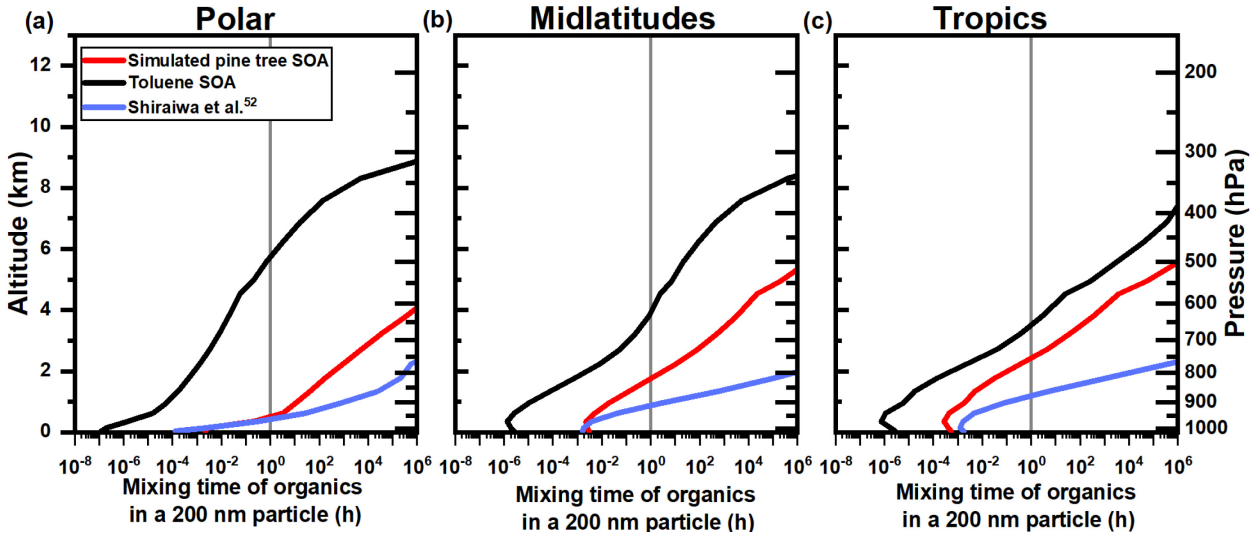

Figure 9. Annual average altitude profiles of the mixing time of organics in a 200 nm particle for a) polar (latitude greater than 66.3° and less than -66.3°), b) midlatitude (66.3°>latitude>23.26° and -66.3°<latitude<-23.26°), and c) tropical (23.26°>latitude>-23.26°) regions for simulated pine tree SOA (red), toluene SOA (black), and SOA from Shiraiwa et al.[52] (blue). The vertical lines are included to highlight a mixing time of 1 h. Average mixing time values were calculated using the average of the log mixing time data as a function of latitude.

In our analysis we focused on a mixing time of 1 h. Typical timescales used in global atmospheric models are often in the range of 0.5-1 h. The overall conclusions reached here do not change if a timescale of 0.5 h was used instead of 1 h (Figure S1 and S2).

3.5 Possible reasons for the difference between the current results and Shiraiwa et al.

The T_g/T values, mixing times of water, and mixing times of organics predicted by Shiraiwa et al.[52] were larger than those predicted here for the same altitude and latitude. These differences could be due to several reasons. For example, the method used to predict viscosities by Shiraiwa et al.[52] was very different than the method used here (see Section 2.4 for details). Several parameters were needed for the predictions by Shiraiwa et al.[52] including the hygroscopicity and Gordon-Taylor constants for the SOA. These parameters each have their own uncertainties, which could lead to an under or over prediction of the viscosity of the SOA. In addition, the parameterization used by Shiraiwa et al.[52] to convert molar mass and O:C to a glass transition temperature had an uncertainty of +/- 15 K for individual components, which

could also lead to an under or over prediction of the viscosity of the SOA at a given temperature and RH, although the uncertainty might be as small as +/- 3 K for SOA mixtures.

In our study, we used experimentally determined viscosity measurements of SOA generated in an environmental chamber. In this case, the SOA was formed during a short time period (less than 2 h), and hence corresponded to fresh SOA. In contrast, the simulations by Shiraiwa et al.[52] took into account atmospheric aging of fresh SOA using a chemistry-climate model. This atmospheric aging could lead to reduced volatilities and higher viscosities, T_g/T values, and mixing times.[46,100–105] In addition, the SOA used to generate the parameterization for the simulated pine tree SOA discussed here was produced with mass concentrations of 50 to 60 μg m^{-3},[58] which was higher than SOA mass concentrations found in the FT. Previous studies have shown that higher mass concentrations could lead to lower viscosities, and hence lower T_g/T values and mixing times.[36,106,107] In contrast, Shiraiwa et al.[52] used a chemical transport model to predict mass concentrations, which was able to reproduce spatial distributions and mass concentrations of SOA measured in the troposphere.[108] The SOA used to generate the parameterization for toluene SOA was produced with mass concentrations of either 60-100 μg m^{-3} or 600-1000 μg m^{-3}, with no dependence of the viscosity on production mass concentration.[48] As a result, it is unknown whether the viscosity would increase at lower mass concentrations for the toluene SOA.

As a proxy of biogenic SOA, we used SOA generated from a mixture of VOCs representative of tree emissions. It is expected that this SOA would be a good proxy for SOA over a boreal forest.[58,61,62] However, it might not be a good proxy for biogenic SOA over all types of biomes because the composition of emitted VOCs varies greatly between different plant functional types.[109] The results from Shiraiwa et al.[52] included emissions from both boreal and temperate forests, which could produce differing results in regions with temperate forests.

Finally, Shiraiwa et al.[52] took into account various emission of VOCs from both anthropogenic and biogenic sources. Conversely, we used a single VOC (toluene) to represent anthropogenic emissions and a mixture of VOCs similar to emissions of VOCs from pine trees to represent biogenic SOA. Differences in the VOCs used to generate SOA in our experiments and the model by Shiraiwa et al.[52] could also lead to differences in viscosities. For example, SOA generated from the photooxidation of isoprene and SOA generated from the ozonolysis of α-pinene gave different viscosities than SOA from pine tree

emissions.[36,58,110] As a result, the predicted viscosities from either study would be dependent on the precursor VOCs used for the SOA, potentially causing different predictions of viscosity.

In conclusion, the differences between the current study and the study by Shiraiwa et al.[52] might be explained by the higher mass concentrations and lack of chemical aging of the SOA used to develop the pine tree SOA parameterization, as well as the VOCs that contributed to the SOA in each study. The differences in methodologies used to predict viscosity might also play a role.

4 Summary, conclusions, implications, and outlook

Parameterizations for viscosity as a function of temperature and RH were developed for simulated pine tree SOA (biogenic SOA proxy) and toluene SOA (anthropogenic SOA proxy) based on room temperature viscosity data. Based on these parameterizations, as well as tropospheric RH and temperature fields, the phase state and mixing times of water and organic molecules in SOA particles were predicted. Some of the key results are summarized and compared with Shiraiwa et al.[52] in Table 1. Based on our results, the glassy state can often occur, and the mixing time of water can often exceed 1 h at altitudes > 6 km. The mixing time of organic molecules can often exceed 1 h throughout most of the FT. The glassy state is not important in the PBL and the mixing time of water and organic molecules is less than 1 h for most of the PBL. The latter conclusion is consistent with previous predictions, field measurements, and laboratory studies of SOA at temperatures and RH values common for the PBL.[43,50,111–115]

The timescale of a typical updraft in the atmosphere is between a few minutes and 1 h.[16] During an updraft, the temperature will decrease and the RH will increase. Due to the long mixing times of water in SOA at altitudes > 6 km, SOA may not be able to reach equilibrium with the surrounding RH during updrafts in this region of the atmosphere. As a result, heterogenous ice nucleation by the glassy state will be more likely since a glassy core is more likely to be able to persist during an updraft in this region of the atmosphere.

Long mixing times of organics in the FT have implications for the long-range transport of pollutants such as polycyclic aromatic hydrocarbons (PAHs). Previous studies have shown that aerosol particles can undergo long-range transport at altitudes of 2-6 km, depending on the latitude and longitude.[116–118] These altitudes correspond to altitudes where the mixing times of organics within SOA can be long. As a result,

pollutant molecules can be trapped within SOA particles during long-range transport, inhibiting their degradation via oxidation.[34,119–122]

The mixing time of organics in SOA is predicted to be less than 1 h for most of the PBL, where the majority of SOA is formed. This means that the assumption of equilibrium partitioning for SOA formation used in global chemical transport models is reasonable for most of the PBL, consistent with previous conclusions.[43,50,52,113,120–122] Equilibrium partitioning for SOA may not be valid in cases where SOA is formed in the FT.[123]

Our results are qualitatively consistent with the findings in Shiraiwa et al.[52], but there are quantitative differences. The T_g/T values, mixing times of water, and mixing times of organics predicted by Shiraiwa et al.[52] were larger than those predicted here for the same altitude and latitude. In addition, the glassy state was predicted to occur at roughly 2 km lower in altitude by Shiraiwa et al.[52] Furthermore, mixing times of organic molecules within SOA were predicted to exceed 1 h at approximately 1 km lower in altitude by Shiraiwa et al.[52] Additional studies are needed to better understand the reasons for these differences.

Both this study and the study by Shiraiwa et al.[52] investigated mixing times within SOA particles with diameters of 200 nm. These calculations could be extended to other particles sizes, and the results would scale as the diameter squared. As a result, larger particles would have longer mixing times and smaller particles would have shorter mixing times. The phase state calculations (i.e. T_g/T values) are independent of the particle size so the predications presented by both studies would apply to all SOA particles in the accumulation mode.

For biogenic SOA, this study focused on simulated healthy pine tree SOA, where the VOC emissions are predominately monoterpenes with a small contribution from sesquiterpenes.[66] However, it has been shown that the VOC emission profile can change when the tree is stressed,[60,66] and the prevalence of plant stress conditions are increasing in frequency and severity.[124–126] The SOA generated from the stress trees has been shown to have a higher viscosity than the healthy trees,[58] meaning that the prevalence of glassy SOA from pine trees could increase in the future.

The biogenic and anthropogenic SOA were considered separately in the current study, whereas SOA in the atmosphere would likely be a mixture of SOA from multiple biogenic sources and anthropogenic sources. To apply the method described in the current study to mixtures, mixing rules for viscosities could

be used.[42,127–129] These mixing rules have been used in the past to predict the viscosity of organic-water and SOA-water mixtures with some success.

To improve predictions of phase state, mixing times of water, and mixing times of organic molecules in SOA particles, laboratory viscosity or diffusion measurements as a function of RH are needed for SOA prepared at lower, more atmospherically relevant mass concentrations. Explicit measurements of viscosity at reduced temperatures are needed as well. In addition, viscosity or diffusion measurements of more oxidized (i.e. aged) SOA are needed to better replicate atmospheric SOA. The current study used simulated pine tree SOA and toluene SOA to represent biogenic SOA and anthropogenic SOA, respectively. Similar studies with other types of SOA are also needed. These experiments will provide a greater understanding of the phase state and mixing times in atmospheric SOA, which will allow for improved predictions of these properties. Other important types of SOA include biomass burning SOA and low volatility isoprene derived epoxydiols (IEPOX)-SOA.[130,131] Although viscosities of primary biomass burning organic aerosol have been estimated based on chemical composition or volatility distributions,[70,105] viscosities of SOA from biomass burning have not been reported in the literature. IEPOX-SOA has been shown to have relatively high viscosity,[130,131] similar or higher than the simulated pine tree SOA discussed here.

Similar to Shiraiwa et al,[52] the results presented here are based on average annual RH and temperature fields. Additional studies are needed to determine how the global distributions of the phase state and mixing times within SOA change with time of day and season. The RH and temperature fields in the free troposphere will depend less on the time of the day than at the surface.[132,133] In the PBL, RH and temperature will vary significantly with the time of day and season, and hence phase state and mixing times within SOA are also expected to vary with time of day and season.[54,134–136]

Table 1: Altitudes at which SOA reaches a glassy state and mixing time of water and organics in SOA are greater than 1 h for different regions of the Earth. Latitudes of -90° and -30° are shown, since these latitudes correspond to the lowest altitudes that SOA reaches a glassy state and mixing time of water and organics in SOA are greater than 1 h for simulated pine tree SOA and toluene SOA, respectively.

SOA Property	**Source of SOA**	**Region of the Earth**				
		-90° latitude	**-30° latitude**	**Tropical**	**Midlatitude**	**Polar**
T_g/T greater than 1	Simulated pine tree SOA (current study)	0 km	4 km	5.5 km	5.25 km	4.25 km
	Shiraiwa et al.[52] (Mostly Biogenic SOA)	0.5 km	2 km	3 km	2.5 km	2.5 km
	Toluene SOA (current study)	8.5 km	5 km	7.25 km	8.5 km	8.75 km
Mixing time of water greater than 1 h in 200 nm SOA	Simulated pine tree SOA (current study)	1.5 km	5.5 km	6.75 km	6.5 km	5 km
	Shiraiwa et al.[52] (Mostly Biogenic SOA)	1 km	5 km	6 km	5.5 km	4.5 km
	Toluene SOA (current study)	8.5 km	8 km	9.5 km	8.75 km	9 km
Mixing time of organics greater than 1 h in 200 nm SOA	Simulated pine tree SOA (current study)	0 km	1.5 km	2.5 km	1.75 km	0.5 km
	Shiraiwa et al.[52] (Mostly Biogenic SOA)	0 km	0.75 km	1 km	1 km	0.5 km
	Toluene SOA (current study)	1.5 km	2.25 km	3.5 km	4 km	5.75 km

ASSOCIATED CONTENT

Supporting Information

The Supporting Information is available free of charge at https://pubs.acs.org/doi/10.1021/acsearthspacechem.XXXXXX.

Viscosity measurements using poke-flow; viscosity measurements using fluorescence recovery after photobleaching; activity based mixing rule derivation; viscosity of water as a function of temperature calculation

Author Information

Corresponding Author

Allan K. Bertram − Department of Chemistry, University of British Columbia, Vancouver, British Columbia V6T 1Z1, Canada; orcid.org/0000-0002-5621-2323; Email: bertram@chem.ubc.ca

Authors

Adrian M. Maclean − Department of Chemistry, University of British Columbia, Vancouver, British Columbia V6T 1Z1, Canada; orcid.org/0000-0003-0901-5287

Ying Li − Institute of Atmospheric Physics, Chinese Academy of Sciences, Beijing, 100029, China; orcid.org/0000-0002-0025-3484

Giuseppe V. Crescenzo − Department of Chemistry, University of British Columbia, Vancouver, British Columbia V6T 1Z1, Canada; orcid.org/0000-0003-0936-3935

Natalie R. Smith − Department of Chemistry, University of California, Irvine, California 92697-2025, United States; orcid.org/0000-0002-9427-1076

Vlassis A. Karydis − Institute of Energy & Climate Research, IEK-8: Troposphere, Forschungszentrum Jülich GmbH, 52428 Jülich, Germany; orcid.org/0000-0002-1616-9746

Alexandra P. Tsimpidi − Institute of Energy & Climate Research, IEK-8: Troposphere, Forschungszentrum Jülich GmbH, 52428 Jülich, Germany and Institute for Environmental Research & Sustainable Development, National Observatory of Athens, 15236 Palea Penteli, Greece; orcid.org/0000-0001-8773-4987

Christopher L. Butenhoff − Dept. of Physics, Portland State University, Portland, Oregon, 97201, USA

Celia L. Faiola – Department of Ecology and Evolutionary Biology and Department of Chemistry, University of California, Irvine, California 92697, United States; orcid.org/0000-0002-4987-023X

Jos Lelieveld –Atmospheric Chemistry Department, Max Planck Institute for Chemistry, 55128 Mainz, Germany and Energy, Environment and Water Research Center, The Cyprus Institute, Nicosia 1645, Cyprus; orcid.org/0000-0001-6307-3846

Sergey A. Nizkorodov − Department of Chemistry, University of California, Irvine, California 92697-2025, United States; orcid.org/0000-0003-0891-0052

Manabu Shiraiwa − Department of Chemistry, University of California, Irvine, California 92697-2025, United States; orcid.org/0000-0003-2532-5373

Acknowledgements

We thank Alexander Laskin, Anusha P. S. Hettiyadura, and Kyla Siemens for their work collecting the mass spectrum of the healthy tree SOA. We thank Jose Jimenez for very helpful discussions during the initial stages of this research. The UBC team was funded by the Natural Science and Engineering Research Council of Canada. NRS thanks the University of California, Irvine Department of Chemistry for support with Rowland Graduate Research Fellowship and US National Science Foundation (grant AGS-1853639). MS thanks the National Science Foundation (AGS-1654104) and the Department of Energy (DE-SC0018349, DE-SC0022139) for funding.

References

(1) Ervens, B.; Turpin, B. J.; Weber, R. J. Secondary Organic Aerosol Formation in Cloud Droplets and Aqueous Particles (AqSOA): A Review of Laboratory, Field and Model Studies. *Atmos. Chem. Phys.* **2011**, *11* (21), 11069–11102. https://doi.org/10.5194/acp-11-11069-2011.

(2) Hallquist, M.; Wenger, J. C.; Baltensperger, U.; Rudich, Y.; Simpson, D.; Claeys, M.; Dommen, J.; Donahue, N. M.; George, C.; Goldstein, A. H.; Hamilton, J. F.; Herrmann, H.; Hoffmann, T.; Iinuma, Y.; Jang, M.; Jenkin, M. E.; Jimenez, J. L.; Kiendler-Scharr, A.; Maenhaut, W.; McFiggans, G.; Mentel, T. F.; Monod, A.; Prévôt, A. S. H.; Seinfeld, J. H.; Surratt, J. D.; Szmigielski, R.; Wildt, J. The Formation, Properties and Impact of Secondary Organic Aerosol: Current and Emerging Issues. *Atmos. Chem. Phys.* **2009**, *9* (14), 5155–5236. https://doi.org/10.5194/acp-9-5155-2009.

(3) *IPCC 2013: Climate Change 2013: The Physical Science Basis. Contribution of Working Group I to the Fifth Assessment Report of the Intergovernmental Panel on Climate Change*; Stocker, T. F., Quin, D., Plattner, G.-K., Tignor, M. M. B., Allen, S. K., Boschung, J., Nauels, A., Xia, Y., Bex, V., Midgley, P. M., Eds.; Cambridge Univ

Press, Cambridge, UK, 2013. https://doi.org/10.1017/CBO9781107415324.

(4) Shiraiwa, M.; Ueda, K.; Pozzer, A.; Lammel, G.; Kampf, C. J.; Fushimi, A.; Enami, S.; Arangio, A. M.; Fröhlich-Nowoisky, J.; Fujitani, Y.; Furuyama, A.; Lakey, P. S. J.; Lelieveld, J.; Lucas, K.; Morino, Y.; Pöschl, U.; Takahama, S.; Takami, A.; Tong, H.; Weber, B.; Yoshino, A.; Sato, K. Aerosol Health Effects from Molecular to Global Scales. *Environ. Sci. Technol.* **2017**, *51* (23), 13545–13567. https://doi.org/10.1021/acs.est.7b04417.

(5) Pope III, C. A.; Dockery, D. D. Health Effects of Fine Particulate Air Pollution: Lines That Connect. *J. Air Waste Manage. Assoc.* **2006**, *56* (May), 709–742. https://doi.org/10.1080/10473289.2006.10464485.

(6) Lelieveld, J.; Evans, J. S.; Fnais, M.; Giannadaki, D.; Pozzer, A. The Contribution of Outdoor Air Pollution Sources to Premature Mortality on a Global Scale. *Nature* **2015**, *525* (7569), 367–371. https://doi.org/10.1038/nature15371.

(7) Cohen, A. J.; Brauer, M.; Burnett, R.; Anderson, H. R.; Frostad, J.; Estep, K.; Balakrishnan, K.; Brunekreef, B.; Dandona, L.; Dandona, R.; Feigin, V.; Freedman, G.; Hubbell, B.; Jobling, A.; Kan, H.; Knibbs, L.; Liu, Y.; Martin, R.; Morawska, L.; Pope, C. A.; Shin, H.; Straif, K.; Shaddick, G.; Thomas, M.; van Dingenen, R.; van Donkelaar, A.; Vos, T.; Murray, C. J. L.; Forouzanfar, M. H. Estimates and 25-Year Trends of the Global Burden of Disease Attributable to Ambient Air Pollution: An Analysis of Data from the Global Burden of Diseases Study 2015. *Lancet* **2017**, *389* (10082), 1907–1918. https://doi.org/10.1016/S0140-6736(17)30505-6.

(8) Lelieveld, J. Clean Air in the Anthropocene. *Faraday Discuss.* **2017**, *200*, 693–703. https://doi.org/10.1039/c7fd90032e.

(9) Koop, T.; Bookhold, J.; Shiraiwa, M.; Pöschl, U. Glass Transition and Phase State of Organic Compounds: Dependency on Molecular Properties and Implications for Secondary Organic Aerosols in the Atmosphere. *Phys. Chem. Chem. Phys.* **2011**, *13* (43), 19238–19255. https://doi.org/10.1039/c1cp22617g.

(10) Ignatius, K.; Kristensen, T. B.; Järvinen, E.; Nichman, L.; Fuchs, C.; Gordon, H.; Herenz, P.; Hoyle, C. R.; Duplissy, J.; Garimella, S.; Dias, A.; Frege, C.; Höppel, N.; Tröstl, J.; Wagner, R.; Yan, C.; Amorim, A.; Baltensperger, U.; Curtius, J.; Donahue, N. M.; Gallagher, M. W.; Kirkby, J.; Kulmala, M.; Möhler, O.; Saathoff, H.; Schnaiter, M.; Tomé, A.; Virtanen, A.; Worsnop, D.; Stratmann, F. Heterogeneous Ice Nucleation of Viscous Secondary Organic Aerosol Produced from Ozonolysis of α-Pinene. *Atmos. Chem. Phys.* **2016**, *16* (10), 6495–6509. https://doi.org/10.5194/acp-16-6495-2016.

(11) Murray, B. J.; Wilson, T. W.; Dobbie, S.; Cui, Z.; Al-Jumur, S. M. R. K.; Möhler, O.; Schnaiter, M.; Wagner, R.; Benz, S.; Niemand, M.; Saathoff, H.; Ebert, V.; Wagner, S.; Kärcher, B. Heterogeneous Nucleation of Ice Particles on Glassy Aerosols under Cirrus Conditions. *Nat. Geosci.* **2010**, *3* (4), 233–237. https://doi.org/10.1038/ngeo817.

(12) Wagner, R.; Möhler, O.; Saathoff, H.; Schnaiter, M.; Skrotzki, J.; Leisner, T.; Wilson, T. W.; Malkin, T. L.; Murray, B. J. Ice Cloud Processing of Ultra-Viscous/Glassy Aerosol Particles Leads to Enhanced Ice Nucleation Ability. *Atmos. Chem. Phys.* **2012**, *12* (18), 8589–8610. https://doi.org/10.5194/acp-12-8589-2012.

(13) Wang, B.; Lambe, A. T.; Massoli, P.; Onasch, T. B.; Davidovits, P.; Worsnop, D. R.; Knopf, D. A. The Deposition Ice Nucleation and Immersion Freezing Potential of Amorphous Secondary Organic Aerosol: Pathways for Ice and

Mixed-Phase Cloud Formation. *J. Geophys. Res.* **2012**, *117* (D16209). https://doi.org/10.1029/2012jd018063.

(14) Knopf, D. A.; Alpert, P. A.; Wang, B. The Role of Organic Aerosol in Atmospheric Ice Nucleation: A Review. *ACS Earth Sp. Chem.* **2018**, *2* (3), 168–202. https://doi.org/10.1021/acsearthspacechem.7b00120.

(15) Wolf, M. J.; Zhang, Y.; Zawadowicz, M. A.; Goodell, M.; Froyd, K.; Freney, E.; Sellegri, K.; Rösch, M.; Cui, T.; Winter, M.; Lacher, L.; Axisa, D.; DeMott, P. J.; Levin, E. J. T.; Gute, E.; Abbatt, J.; Koss, A.; Kroll, J. H.; Surratt, J. D.; Cziczo, D. J. A Biogenic Secondary Organic Aerosol Source of Cirrus Ice Nucleating Particles. *Nat. Commun.* **2020**, *11* (1). https://doi.org/10.1038/s41467-020-18424-6.

(16) Berkemeier, T.; Shiraiwa, M.; Pöschl, U.; Koop, T. Competition between Water Uptake and Ice Nucleation by Glassy Organic Aerosol Particles. *Atmos. Chem. Phys.* **2014**, *14* (22), 12513–12531. https://doi.org/10.5194/acp-14-12513-2014.

(17) Shiraiwa, M.; Seinfeld, J. H. Equilibration Timescale of Atmospheric Secondary Organic Aerosol Partitioning. *Geophys. Res. Lett.* **2012**, *39* (L24801). https://doi.org/10.1029/2012gl054008.

(18) Zaveri, R. A.; Easter, R. C.; Shilling, J. E.; Seinfeld, J. H. Modeling Kinetic Partitioning of Secondary Organic Aerosol and Size Distribution Dynamics: Representing Effects of Volatility, Phase State, and Particle-Phase Reaction. *Atmos. Chem. Phys.* **2014**, *14* (10), 5153–5181. https://doi.org/10.5194/acp-14-5153-2014.

(19) Zaveri, R. A.; Shilling, J. E.; Zelenyuk, A.; Liu, J.; Bell, D. M.; D'Ambro, E. L.; Gaston, C. J.; Thornton, J. A.; Laskin, A.; Lin, P.; Wilson, J.; Easter, R. C.; Wang, J.; Bertram, A. K.; Martin, S. T.; Seinfeld, J. H.; Worsnop, D. R. Growth Kinetics and Size Distribution Dynamics of Viscous Secondary Organic Aerosol. *Environ. Sci. Technol.* **2018**, *52* (3), 1191–1199. https://doi.org/10.1021/acs.est.7b04623.

(20) Shiraiwa, M.; Yee, L. D.; Schilling, K. A.; Loza, C. L.; Craven, J. S.; Zuend, A.; Ziemann, P. J.; Seinfeld, J. H. Size Distribution Dynamics Reveal Particle-Phase Chemistry in Organic Aerosol Formation. *Proc. Natl. Acad. Sci. U. S. A.* **2013**, *110* (29), 11746–11750. https://doi.org/10.1073/pnas.1307501110.

(21) Kim, Y.; Sartelet, K.; Couvidat, F. Modeling the Effect of Non-Ideality, Dynamic Mass Transfer and Viscosity on SOA Formation in a 3-D Air Quality Model. *Atmos. Chem. Phys.* **2019**, *19* (2), 1241–1261. https://doi.org/10.5194/acp-19-1241-2019.

(22) Yli-Juuti, T.; Pajunoja, A.; Tikkanen, O. P.; Buchholz, A.; Faiola, C.; Väisänen, O.; Hao, L.; Kari, E.; Peräkylä, O.; Garmash, O.; Shiraiwa, M.; Ehn, M.; Lehtinen, K.; Virtanen, A. Factors Controlling the Evaporation of Secondary Organic Aerosol from α-Pinene Ozonolysis. *Geophys. Res. Lett.* **2017**, *44* (5), 2562–2570. https://doi.org/10.1002/2016GL072364.

(23) Zhang, Y.; Chen, Y.; Lambe, A. T.; Olson, N. E.; Lei, Z.; Craig, R. L.; Zhang, Z.; Gold, A.; Onasch, T. B.; Jayne, J. T.; Worsnop, D. R.; Gaston, C. J.; Thornton, J. A.; Vizuete, W.; Ault, A. P.; Surratt, J. D. Effect of the Aerosol-Phase State on Secondary Organic Aerosol Formation from the Reactive Uptake of Isoprene-Derived Epoxydiols (IEPOX). *Environ. Sci. Technol. Lett.* **2018**, *5* (3), 167–174. https://doi.org/10.1021/acs.estlett.8b00044.

(24) Steimer, S. S.; Lampimaki, M.; Coz, E.; Grzinic, G.; Ammann, M. The Influence of Physical State on Shikimic Acid

Ozonolysis: A Case for in Situ Microspectroscopy. *Atmos. Chem. Phys.* **2014**, *14* (19), 10761–10772. https://doi.org/10.5194/acp-14-10761-2014.

(25) Houle, F. A.; Hinsberg, W. D.; Wilson, K. R. Oxidation of a Model Alkane Aerosol by OH Radical: The Emergent Nature of Reactive Uptake. *Phys. Chem. Chem. Phys.* **2015**, *17* (6), 4412–4423. https://doi.org/10.1039/c4cp05093b.

(26) Liu, P.; Li, Y. J.; Wang, Y.; Bateman, A. P.; Zhang, Y.; Gong, Z.; Bertram, A. K.; Martin, S. T. Highly Viscous States Affect the Browning of Atmospheric Organic Particulate Matter. *ACS Cent. Sci.* **2018**, *4* (2), 207–215. https://doi.org/10.1021/acscentsci.7b00452.

(27) Li, Z.; Smith, K. A.; Cappa, C. D. Influence of Relative Humidity on the Heterogeneous Oxidation of Secondary Organic Aerosol. *Atmos. Chem. Phys.* **2018**, *18* (19), 14585–14608. https://doi.org/10.5194/acp-18-14585-2018.

(28) Hinks, M. L.; Brady, M. V; Lignell, H.; Song, M. J.; Grayson, J. W.; Bertram, A. K.; Lin, P.; Laskin, A.; Laskin, J.; Nizkorodov, S. A. Effect of Viscosity on Photodegradation Rates in Complex Secondary Organic Aerosol Materials. *Phys. Chem. Chem. Phys.* **2016**, *18* (13), 8785–8793. https://doi.org/10.1039/c5cp05226b.

(29) Shiraiwa, M.; Ammann, M.; Koop, T.; Pöschl, U. Gas Uptake and Chemical Aging of Semisolid Organic Aerosol Particles. *Proc. Natl. Acad. Sci. U. S. A.* **2011**, *108* (27), 11003–11008. https://doi.org/10.1073/pnas.1103045108.

(30) Berkemeier, T.; Steimer, S. S.; Krieger, U. K.; Peter, T.; Pöschl, U.; Ammann, M.; Shiraiwa, M. Ozone Uptake on Glassy, Semi-Solid and Liquid Organic Matter and the Role of Reactive Oxygen Intermediates in Atmospheric Aerosol Chemistry. *Phys. Chem. Chem. Phys.* **2016**, *18* (18), 12662–12674. https://doi.org/10.1039/c6cp00634e.

(31) Li, Y. J.; Liu, P. F.; Gong, Z. H.; Wang, Y.; Bateman, A. P.; Bergoend, C.; Bertram, A. K.; Martin, S. T. Chemical Reactivity and Liquid/Nonliquid States of Secondary Organic Material. *Environ. Sci. Technol.* **2015**, *49* (22), 13264–13274. https://doi.org/10.1021/acs.est.5b03392.

(32) Li, J.; Forrester, S. M.; Knopf, D. A. Heterogeneous Oxidation of Amorphous Organic Aerosol Surrogates by O3, NO3, and OH at Typical Tropospheric Temperatures. *Atmos. Chem. Phys.* **2020**, *20* (10), 6055–6080. https://doi.org/10.5194/acp-20-6055-2020.

(33) Zhao, Z.; Tolentino, R.; Lee, J.; Vuong, A.; Yang, X.; Zhang, H. Interfacial Dimerization by Organic Raical Reactions Uring Heterogeneous Oxiative Aging of Oxygenate Organic Aerosols. *J. Phys. Chem. A* **2019**, *123* (50), 10782–10792. https://doi.org/10.1021/acs.jpca.9b10779.

(34) Zhou, S.; Shiraiwa, M.; McWhinney, R. D.; Pöschl, U.; Abbatt, J. P. D. Kinetic Limitations in Gas-Particle Reactions Arising from Slow Diffusion in Secondary Organic Aerosol. *Faraday Discuss.* **2013**, *165*, 391–406. https://doi.org/10.1039/c3fd00030c.

(35) Abramson, E.; Imre, D.; Beranek, J.; Wilson, J.; Zelenyuk, A. Experimental Determination of Chemical Diffusion within Secondary Organic Aerosol Particles. *Phys. Chem. Chem. Phys.* **2013**, *15* (8), 2983–2991. https://doi.org/10.1039/C2CP44013J.

(36) Grayson, J. W.; Zhang, Y.; Mutzel, A.; Renbaum-Wolff, L.; Böge, O.; Kamal, S.; Herrmann, H.; Martin, S. T.; Bertram, A. K. Effect of Varying Experimental Conditions on the Viscosity of α-Pinene Derived Secondary Organic

Material. *Atmos. Chem. Phys.* **2016**, *16* (10), 6027–6040. https://doi.org/10.5194/acp-16-6027-2016.

(37) Kiland, K. J.; Maclean, A. M.; Kamal, S.; Bertram, A. K. Diffusion of Organic Molecules as a Function of Temperature in a Sucrose Matrix (a Proxy for Secondary Organic Aerosol). *J. Phys. Chem. Lett.* **2019**, *10* (19), 5902–5908. https://doi.org/10.1021/acs.jpclett.9b02182.

(38) Evoy, E.; Kamal, S.; Patey, G. N.; Martin, S. T.; Bertram, A. K. Unified Description of Diffusion Coefficients from Small to Large Molecules in Organic-Water Mixtures. *J. Phys. Chem. A* **2020**, *124* (11), 2301–2308. https://doi.org/10.1021/acs.jpca.9b11271.

(39) Evoy, E.; Maclean, A. M.; Rovelli, G.; Li, Y.; Tsimpidi, A. P.; Karydis, V. A.; Kamal, S.; Lelieveld, J.; Shiraiwa, M.; Reid, J. P.; Bertram, A. K. Predictions of Diffusion Rates of Large Organic Molecules in Secondary Organic Aerosols Using the Stokes-Einstein and Fractional Stokes-Einstein Relations. *Atmos. Chem. Phys.* **2019**, *19* (15), 10073–10085. https://doi.org/10.5194/acp-19-10073-2019.

(40) Bastelberger, S.; Krieger, U. K.; Luo, B.; Peter, T. Diffusivity Measurements of Volatile Organics in Levitated Viscous Aerosol Particles. *Atmos. Chem. Phys.* **2017**, *17* (13), 8453–8471. https://doi.org/10.5194/acp-17-8453-2017.

(41) Reid, J. P.; Bertram, A. K.; Topping, D. O.; Laskin, A.; Martin, S. T.; Petters, M. D.; Pope, F. D.; Rovelli, G. The Viscosity of Atmospherically Relevant Organic Particles. *Nat. Commun.* **2018**, *9* (1), 1–14. https://doi.org/10.1038/s41467-018-03027-z.

(42) Gervasi, N. R.; Topping, D. O.; Zuend, A. A Predictive Group-Contribution Model for the Viscosity of Aqueous Organic Aerosol. *Atmos. Chem. Phys.* **2020**, *20* (5), 2987–3008. https://doi.org/10.5194/acp-20-2987-2020.

(43) Liu, P.; Li, Y. J.; Wang, Y.; Gilles, M. K.; Zaveri, R. A.; Bertram, A. K.; Martin, S. T. Lability of Secondary Organic Particulate Matter. *Proc. Natl. Acad. Sci. U. S. A.* **2016**, *113* (45), 12643–12648. https://doi.org/10.1073/pnas.1603138113.

(44) Renbaum-Wolff, L.; Grayson, J. W.; Bateman, A. P.; Kuwata, M.; Sellier, M.; Murray, B. J.; Shilling, J. E.; Martin, S. T.; Bertram, A. K. Viscosity of α-Pinene Secondary Organic Material and Implications for Particle Growth and Reactivity. *Proc. Natl. Acad. Sci. U. S. A.* **2013**, *110* (20), 8014–8019. https://doi.org/10.1073/pnas.1219548110.

(45) Zobrist, B.; Soonsin, V.; Luo, B. P.; Krieger, U. K.; Marcolli, C.; Peter, T.; Koop, T. Ultra-Slow Water Diffusion in Aqueous Sucrose Glasses. *Phys. Chem. Chem. Phys.* **2011**, *13* (8), 3514–3526. https://doi.org/10.1039/c0cp01273d.

(46) Zhang, Y.; Nichman, L.; Spencer, P.; Jung, J. I.; Lee, A.; Heffernan, B. K.; Gold, A.; Zhang, Z.; Chen, Y.; Canagaratna, M. R.; Jayne, J. T.; Worsnop, D. R.; Onasch, T. B.; Surratt, J. D.; Chandler, D.; Davidovits, P.; Kolb, C. E. The Cooling Rate- And Volatility-Dependent Glass-Forming Properties of Organic Aerosols Measured by Broadband Dielectric Spectroscopy. *Environ. Sci. Technol.* **2019**, *53* (21), 12366–12378. https://doi.org/10.1021/acs.est.9b03317.

(47) Li, Y.; Shiraiwa, M. Timescales of Secondary Organic Aerosols to Reach Equilibrium at Various Temperatures and Relative Humidities. *Atmos. Chem. Phys.* **2019**, *19* (9), 5959–5971. https://doi.org/10.5194/acp-19-5959-2019.

(48) Song, M. J.; Liu, P. F. F.; Hanna, S. J.; Zaveri, R. A.; Potter, K.; You, Y.; Martin, S. T.; Bertram, A. K. Relative Humidity-Dependent Viscosity of Secondary Organic Material from Toluene Photo-Oxidation and Possible

Implications for Organic Particulate Matter over Megacities. *Atmos. Chem. Phys.* **2016**, *16* (14), 8817–8830. https://doi.org/10.5194/acp-16-8817-2016.

(49) Virtanen, A.; Joutsensaari, J.; Koop, T.; Kannosto, J.; Yli-Pirilä, P.; Leskinen, J.; Mäkelä, J. M.; Holopainen, J. K.; Pöschl, U.; Kulmala, M.; Worsnop, D. R.; Laaksonen, A. An Amorphous Solid State of Biogenic Secondary Organic Aerosol Particles. *Nature* **2010**, *467* (7317), 824–827. https://doi.org/10.1038/nature09455.

(50) Maclean, A. M.; Butenhoff, C. L.; Grayson, J. W.; Barsanti, K.; Jimenez, J. L.; Bertram, A. K. Mixing Times of Organic Molecules within Secondary Organic Aerosol Particles: A Global Planetary Boundary Layer Perspective. *Atmos. Chem. Phys.* **2017**, *17* (21), 13037–13048. https://doi.org/10.5194/acp-17-13037-2017.

(51) Wallace, J. M.; Hobbs, P. V. *Atmospheric Science: An Introductory Survery*; Academic Press: Burlington , MA, 2006.

(52) Shiraiwa, M.; Li, Y.; Tsimpidi, A. P.; Karydis, V. A.; Berkemeier, T.; Pandis, S. N.; Lelieveld, J.; Koop, T.; Pöschl, U. Global Distribution of Particle Phase State in Atmospheric Secondary Organic Aerosols. *Nat. Commun.* **2017**. https://doi.org/10.1038/ncomms15002.

(53) Schmedding, R.; Rasool, Q. Z.; Zhang, Y.; Pye, H. O. T.; Zhang, H.; Chen, Y.; Surratt, J. D.; Lopez-Hilfiker, F. D.; Thornton, J. A.; Goldstein, A. H.; Vizuete, W. Predicting Secondary Organic Aerosol Phase State and Viscosity and Its Effect on Multiphase Chemistry in a Regional-Scale Air Quality Model. *Atmos. Chem. Phys.* **2020**, *20* (13), 8201–8225. https://doi.org/10.5194/acp-20-8201-2020.

(54) Li, Y.; Carlton, A. G.; Shiraiwa, M. Diurnal and Seasonal Variations in the Phase State of Secondary Organic Aerosol Material over the Contiguous US Simulated in CMAQ. *ACS Earth Sp. Chem.* **2021**, *5* (8), 1971–1982. https://doi.org/10.1021/acsearthspacechem.1c00094.

(55) Riipinen, I.; Pierce, J. R.; Yli-Juuti, T.; Nieminen, T.; Hakkinen, S.; Ehn, M.; Junninen, H.; Lehtipalo, K.; Petaja, T.; Slowik, J.; Chang, R.; Shantz, N. C.; Abbatt, J.; Leaitch, W. R.; Kerminen, V. M.; Worsnop, D. R.; Pandis, S. N.; Donahue, N. M.; Kulmala, M. Organic Condensation: A Vital Link Connecting Aerosol Formation to Cloud Condensation Nuclei (CCN) Concentrations. *Atmos. Chem. Phys.* **2011**, *11* (8), 3865–3878. https://doi.org/10.5194/acp-11-3865-2011.

(56) Pöschl, U.; Martin, S. T.; Sinha, B.; Chen, Q.; Gunthe, S. S.; Huffman, J. A.; Borrmann, S.; Farmer, D. K.; Garland, R. M.; Helas, G.; Jimenez, J. L.; King, S. M.; Manzi, A.; Mikhailov, E.; Pauliquevis, T.; Petters, M. D.; Prenni, A. J.; Roldin, P.; Rose, D.; Schneider, J.; Su, H.; Zorn, S. R.; Artaxo, P.; Andreae, M. O. Rainforest Aerosols as Biogenic Nuclei of Clouds and Precipitation in the Amazon. *Science* **2010**, *329* (5998), 1513–1516. https://doi.org/10.1126/science.1191056.

(57) Martin, S. T.; Andreae, M. O.; Althausen, D.; Artaxo, P.; Baars, H.; Borrmann, S.; Chen, Q.; Farmer, D. K.; Guenther, A.; Gunthe, S. S.; Jimenez, J. L.; Karl, T.; Longo, K.; Manzi, A.; Müller, T.; Pauliquevis, T.; Petters, M. D.; Prenni, A. J.; Pöschl, U.; Rizzo, L. V.; Schneider, J.; Smith, J. N.; Swietlicki, E.; Tota, J.; Wang, J.; Wiedensohler, A.; Zorn, S. R. An Overview of the Amazonian Aerosol Characterization Experiment 2008 (AMAZE-08). *Atmos. Chem. Phys.* **2010**, *10* (23), 11415–11438. https://doi.org/10.5194/acp-10-11415-2010.

(58) Smith, N. R.; Crescenzo, G. V.; Huang, Y.; Hettiyadura, A. P. S.; Siemens, K.; Li, Y.; Faiola, C. L.; Laskin, A.; Shiraiwa, M.; Bertram, A. K.; Nizkorodov, S. A. Viscosity and Liquid–Liquid Phase Separation in Healthy and Stressed Plant SOA. *Environ. Sci. Atmos.* **2021**, *1* (3), 140–153. https://doi.org/10.1039/d0ea00020e.

(59) Crittenden, J. C.; Trussel, R. R.; Hand, D. W.; Howe, K. J.; Tchobanoglous, G. *MWH's Water Treatment*; John Wiley and Sons, 2012.

(60) Faiola, C. L.; Pullinen, I.; Buchholz, A.; Khalaj, F.; Ylisirniö, A.; Kari, E.; Miettinen, P.; Holopainen, J. K.; Kivimäenpää, M.; Schobesberger, S.; Yli-Juuti, T.; Virtanen, A. Secondary Organic Aerosol Formation from Healthy and Aphid-Stressed Scots Pine Emissions. *ACS Earth Sp. Chem.* **2019**, *3* (9), 1756–1772. https://doi.org/10.1021/acsearthspacechem.9b00118.

(61) Lundqvist, L.; Ahlström, M. A.; Petter Axelsson, E.; Mörling, T.; Valinger, E. Multi-Layered Scots Pine Forests in Boreal Sweden Result from Mass Regeneration and Size Stratification. *For. Ecol. Manage.* **2019**, *441* (March), 176–181. https://doi.org/10.1016/j.foreco.2019.03.044.

(62) Boratyński, A. *Genetics of Scots Pine*; Giertych, M., Mátyás, C., Eds.; Elsevier: Budapest, 1991.

(63) Ylisirniö, A.; Buchholz, A.; Mohr, C.; Li, Z.; Barreira, L.; Lambe, A.; Faiola, C.; Kari, E.; Yli-Juuti, T.; Nizkorodov, S. A.; Worsnop, D. R.; Virtanen, A.; Schobesberger, S. Composition and Volatility of Secondary Organic Aerosol (SOA) Formed from Oxidation of Real Tree Emissions Compared to Simplified Volatile Organic Compound (VOC) Systems. *Atmos. Chem. Phys.* **2020**, *20* (9), 5629–5644. https://doi.org/10.5194/acp-20-5629-2020.

(64) Ahlberg, E.; Falk, J.; Eriksson, A.; Holst, T.; Brune, W. H.; Kristensson, A.; Roldin, P.; Svenningsson, B. Secondary Organic Aerosol from VOC Mixtures in an Oxidation Flow Reactor. *Atmos. Environ.* **2017**, *161*, 210–220. https://doi.org/10.1016/j.atmosenv.2017.05.005.

(65) McFiggans, G.; Mentel, T. F.; Wildt, J.; Pullinen, I.; Kang, S.; Kleist, E.; Schmitt, S.; Springer, M.; Tillmann, R.; Wu, C.; Zhao, D.; Hallquist, M.; Faxon, C.; Le Breton, M.; Hallquist, Å. M.; Simpson, D.; Bergström, R.; Jenkin, M. E.; Ehn, M.; Thornton, J. A.; Alfarra, M. R.; Bannan, T. J.; Percival, C. J.; Priestley, M.; Topping, D.; Kiendler-Scharr, A. Secondary Organic Aerosol Reduced by Mixture of Atmospheric Vapours. *Nature* **2019**, *565* (7741), 587–593. https://doi.org/10.1038/s41586-018-0871-y.

(66) Faiola, C. L.; Buchholz, A.; Kari, E.; Yli-Pirilä, P.; Holopainen, J. K.; Kivimäenpää, M.; Miettinen, P.; Worsnop, D. R.; Lehtinen, K. E. J.; Guenther, A. B.; Virtanen, A. Terpene Composition Complexity Controls Secondary Organic Aerosol Yields from Scots Pine Volatile Emissions. *Sci. Rep.* **2018**, *8* (1), 1–13. https://doi.org/10.1038/s41598-018-21045-1.

(67) Angell, C. A. Relaxation in Liquids, Polymers and Plastic Crystals - Strong/Fragile Patterns and Problems. *J. Non. Cryst. Solids* **1991**, *133*, 13–31.

(68) Angell, C. A. Liquid Fragility and the Glass Transition in Water and Aqueous Solutions. *Chem. Rev.* **2002**, *102* (8), 2627–2650. https://doi.org/10.1021/cr000689q.

(69) Angell, C. A. Entropy and Fragility in Supercooling Liquids. *J. Res. Natl. Inst. Stand. Technol.* **1997**, *102* (2), 171–

181. https://doi.org/10.6028/jres.102.013.

(70) DeRieux, W.-S. W.; Li, Y.; Lin, P.; Laskin, J.; Laskin, A.; Bertram, A. K.; Nizkorodov, S. A.; Shiraiwa, M. Predicting the Glass Transition Temperature and Viscosity of Secondary Organic Material Using Molecular Composition. *Atmos. Chem. Phys.* **2018**, *18* (9), 6331–6351. https://doi.org/10.5194/acp-18-6331-2018.

(71) Marsh, A.; Petters, S. S.; Rothfuss, N. E.; Rovelli, G.; Song, Y. C.; Reid, J. P.; Petters, M. D. Amorphous Phase State Diagrams and Viscosity of Ternary Aqueous Organic/Organic and Inorganic/Organic Mixtures. *Phys. Chem. Chem. Phys.* **2018**, *20* (22), 15086–15097. https://doi.org/10.1039/c8cp00760h.

(72) Rothfuss, N. E.; Petters, M. D. Characterization of the Temperature and Humidity-Dependent Phase Diagram of Amorphous Nanoscale Organic Aerosols. *Phys. Chem. Chem. Phys.* **2017**, *19*, 6532–6545. https://doi.org/10.1039/C6CP08593H.

(73) Longinotti, M. P.; Corti, H. R. Viscosity of Concentrated Sucrose and Trehalose Aqueous Solutions Including the Supercooled Regime. *J. Phys. Chem. Ref. Data* **2008**, *37* (3), 1503–1515. https://doi.org/10.1063/1.2932114.

(74) Kasparoglu, S.; Li, Y.; Shiraiwa, M.; Petters, M. Toward Closure between Predicted and Observed Particle Viscosity over a Wide Range Temperature and Relative Humidity. *Atmos. Chem. Phys.* **2020**, 1–22. https://doi.org/10.5194/acp-2020-768.

(75) de Gouw, J. A.; Brock, C. A.; Atlas, E. L.; Bates, T. S.; Fehsenfeld, F. C.; Goldan, P. D.; Holloway, J. S.; Kuster, W. C.; Lerner, B. M.; Matthew, B. M.; Middlebrook, A. M.; Onasch, T. B.; Peltier, R. E.; Quinn, P. K.; Senff, C. J.; Stohl, A.; Sullivan, A. P.; Trainer, M.; Warneke, C.; Weber, R. J.; Williams, E. J. Sources of Particulate Matter in the Northeastern United States in Summer: 1. Direct Emissions and Secondary Formation of Organic Matter in Urban Plumes. *J. Geophys. Res.* **2008**, *113* (8), 1–19. https://doi.org/10.1029/2007JD009243.

(76) Gao, Y.; Wang, H.; Zhang, X.; Jing, S.; Peng, Y.; Qiao, L.; Zhou, M.; Huang, D. D.; Wang, Q.; Li, X.; Li, L.; Feng, J.; Ma, Y.; Li, Y. Estimating Secondary Organic Aerosol Production from Toluene Photochemistry in a Megacity of China. *Environ. Sci. Technol.* **2019**, *53* (15), 8664–8671. https://doi.org/10.1021/acs.est.9b00651.

(77) Pandis, S. N.; Harley, R. A.; Cass, G. R.; Seinfeld, J. H. Secondary Organic Aerosol Formation and Transport. *Atmos. Environ. Part A, Gen. Top.* **1992**, *26* (13), 2269–2282. https://doi.org/10.1016/0960-1686(92)90358-R.

(78) Robinson, E. S.; Saleh, R.; Donahue, N. M. Organic Aerosol Mixing Observed by Single-Particle Mass Spectrometry. *J. Phys. Chem. A* **2013**, *117* (51), 13935–13945. https://doi.org/10.1021/jp405789t.

(79) Song, M.; Maclean, A. M.; Huang, Y.; Smith, N. R.; Blair, S. L.; Laskin, J.; Laskin, A.; DeRieux, W.-S. W.; Li, Y.; Shiraiwa, M.; Nizkorodov, S. A.; Bertram, A. K. Liquid-Liquid Phase Separation and Viscosity within Secondary Organic Aerosol Generated from Diesel Fuel Vapors. *Atmos. Chem. Phys.* **2019**, *19*, 12515–12529. https://doi.org/10.5194/acp-2019-367.

(80) Gentner, D. R.; Isaacman, G.; Worton, D. R.; Chan, A. W. H.; Dallmann, T. R.; Davis, L.; Liu, S.; Day, D. A.; Russell, L. M.; Wilson, K. R.; Weber, R.; Guha, A.; Harley, R. A.; Goldstein, A. H. Elucidating Secondary Organic Aerosol from Diesel and Gasoline Vehicles through Detailed Characterization of Organic Carbon Emissions. *Proc. Natl. Acad.*

Sci. U. S. A. **2012**, *109* (45), 18318–18323. https://doi.org/10.1073/pnas.1212272109.

(81) Odum, J. R.; Jungkamp, T. P. W.; Griffin, R. J.; Flagan, R. C.; Seinfeld, J. H. The Atmospheric Aerosol-Forming Potential of Whole Gasoline Vapor. *Science (80-.).* **1997**, *276* (5309), 96–99. https://doi.org/10.1126/science.276.5309.96.

(82) Velasco, E.; Lamb, B.; Westberg, H.; Allwine, E.; Sosa, G.; Arriaga-Colina, J. L.; Jobson, B. T.; Alexander, M. L.; Prazeller, P.; Knighton, W. B.; Rogers, T. M.; Grutter, M.; Herndon, S. C.; Kolb, C. E.; Zavala, M.; De Foy, B.; Volkamer, R.; Molina, L. T.; Molina, M. J. Distribution, Magnitudes, Reactivities, Ratios and Diurnal Patterns of Volatile Organic Compounds in the Valley of Mexico during the MCMA 2002 & 2003 Field Campaigns. *Atmos. Chem. Phys.* **2007**, *7* (2), 329–353. https://doi.org/10.5194/acp-7-329-2007.

(83) Velasco, E.; Pressley, S.; Grivicke, R.; Allwine, E.; Coons, T.; Foster, W.; Jobson, B. T.; Westberg, H.; Ramos, R.; Hernández, F.; Molina, L. T.; Lamb, B. Eddy Covariance Flux Measurements of Pollutant Gases in Urban Mexico City. *Atmos. Chem. Phys.* **2009**, *9* (19), 7325–7342. https://doi.org/10.5194/acp-9-7325-2009.

(84) Saathoff, H.; Naumann, K.-H.; Moehler, O.; Jonsson, A. M.; Hallquist, M.; Kiendler-Scharr, A.; Mentel, T. F.; Tillmann, R.; Schurath, U. Temperature Dependence of Yields of Secondary Organic Aerosols from the Ozonolysis of Alpha-Pinene and Limonene. *Atmos. Chem. Phys.* **2009**, *9* (5), 1551–1577. https://doi.org/10.5194/acp-9-1551-2009.

(85) Li, Y. J.; Chen, Q.; Guzman, M. I.; Chan, C. K.; Martin, S. T. Second-Generation Products Contribute Substantially to the Particle-Phase Organic Material Produced by β-Caryophyllene Ozonolysis. *Atmos. Chem. Phys.* **2011**, *11* (1), 121–132. https://doi.org/10.5194/acp-11-121-2011.

(86) Hinks, M. L.; Montoya-Aguilera, J.; Ellison, L.; Lin, P.; Laskin, A.; Laskin, J.; Shiraiwa, M.; Dabdub, D.; Nizkorodov, S. A. Effect of Relative Humidity on the Composition of Secondary Organic Aerosol from the Oxidation of Toluene. *Atmos. Chem. Phys.* **2018**, *18* (3), 1643–1652. https://doi.org/10.5194/acp-18-1643-2018.

(87) Malloy, Q. G. J.; Nakao, S.; Qi, L.; Austin, R.; Stothers, C.; Hagino, H.; Cocker, D. R. Real-Time Aerosol Density Determination Utilizing a Modified Scanning Mobility Particle Sizer Aerosol Particle Mass Analyzer System. *Aerosol Sci. Technol.* **2009**, *43* (7), 673–678. https://doi.org/10.1080/02786820902832960.

(88) Tasoglou, A.; Pandis, S. N. Formation and Chemical Aging of Secondary Organic Aerosol during the β -Caryophyllene Oxidation. *Atmos. Chem. Phys.* **2015**, *15*, 6035–6046. https://doi.org/10.5194/acp-15-6035-2015.

(89) Cross, E. S.; Slowik, J. G.; Davidovits, P.; Allan, J. D.; Worsnop, D. R.; Jayne, J. T.; Lewis, D. K.; Canagaratna, M.; Onasch, T. B. Laboratory and Ambient Particle Density Determinations Using Light Scattering in Conjunction with Aerosol Mass Spectrometry. *Aerosol Sci. Technol.* **2007**, *41* (4), 343–359. https://doi.org/10.1080/02786820701199736.

(90) Bahreini, R.; Keywood, M. D.; Ng, N. L.; Varutbangkul, V.; Gao, S.; Flagan, R. C.; Seinfeld, J. H.; Worsnop, D. R.; Jimenez, J. L. Measurements of Secondary Organic Aerosol from Oxidation of Cycloalkenes, Terpenes, and m-Xylene Using an Aerodyne Aerosol Mass Spectrometer. *Environ. Sci. Technol.* **2005**, *39* (15), 5674–5688.

https://doi.org/10.1021/es048061a.

(91) Ng, N. L.; Kroll, J. H.; Chan, A. W. H.; Chhabra, P. S.; Flagan, R. C.; Ng, N. L.; Kroll, J. H.; Chan, A. W. H.; Chhabra, P. S.; Flagan, R. C. Secondary Organic Aerosol Formation from M-Xylene , Toluene , and Benzene. **2007**.

(92) Seinfeld, J. H.; Pandis, S. N. *Atmospheric Chemistry and Physics*, 2nd Ed.; John Wiley and Sons: Hoboken, NJ, 2006.

(93) Price, H. C.; Mattsson, J.; Murray, B. J. Sucrose Diffusion in Aqueous Solution. *Phys. Chem. Chem. Phys.* **2016**, *18* (28), 19207–19216. https://doi.org/10.1039/C6CP03238A.

(94) Hallett, J. The Temperature Dependence of the Viscosity of Supercooled Water. *Proc. Phys. Soc.* **1963**, *82* (6), 1046–1050. https://doi.org/10.1088/0370-1328/82/6/326.

(95) Tsimpidi, A. P.; Karydis, V. A.; Pozzer, A.; Pandis, S. N.; Lelieveld, J. ORACLE (v1.0): Module to Simulate the Organic Aerosol Composition and Evolution in the Atmosphere. *Geosci. Model Dev.* **2014**, *7* (6), 3153–3172. https://doi.org/10.5194/gmd-7-3153-2014.

(96) Tsimpidi, A. P.; Karydis, V. A.; Pozzer, A.; Pandis, S. N.; Lelieveld, J. ORACLE 2-D (v2.0): An Efficient Module to Compute the Volatility and Oxygen Content of Organic Aerosol with a Global Chemistry-Climate Model. *Geosci. Model Dev.* **2018**, *11* (8), 3369–3389. https://doi.org/10.5194/gmd-11-3369-2018.

(97) Shiraiwa, M.; Berkemeier, T.; Schilling-Fahnestock, K. A.; Seinfeld, J. H.; Poeschl, U. Molecular Corridors and Kinetic Regimes in the Multiphase Chemical Evolution of Secondary Organic Aerosol. *Atmos. Chem. Phys.* **2014**, *14* (16), 8323–8341. https://doi.org/10.5194/acp-14-8323-2014.

(98) Filippone, A. *Flight Performance of Fixed and Rotary Wing Aircraft*; Elsevier Ltd: Oxford, 2006.

(99) Spracklen, D. V; Jimenez, J. L.; Carslaw, K. S.; Worsnop, D. R.; Evans, M. J.; Mann, G. W.; Zhang, Q.; Canagaratna, M. R.; Allan, J.; Coe, H.; McFiggans, G.; Rap, A.; Forster, P. Aerosol Mass Spectrometer Constraint on the Global Secondary Organic Aerosol Budget. *Atmos. Chem. Phys.* **2011**, *11* (23), 12109–12136. https://doi.org/10.5194/acp-11-12109-2011.

(100) Athanasiadis, A.; Fitzgerald, C.; Davidson, N. M.; Giorio, C.; Botchway, S. W.; Ward, A. D.; Kalberer, M.; Pope, F. D.; Kuimova, M. K. Dynamic Viscosity Mapping of the Oxidation of Squalene Aerosol Particles. *Phys. Chem. Chem. Phys.* **2016**, *18* (44), 30385–30393. https://doi.org/10.1039/c6cp05674a.

(101) Hosny, N. A.; Fitzgerald, C.; Vyšniauskas, A.; Athanasiadis, A.; Berkemeier, T.; Uygur, N.; Pöschl, U.; Shiraiwa, M.; Kalberer, M.; Pope, F. D.; Kuimova, M. K. Direct Imaging of Changes in Aerosol Particle Viscosity upon Hydration and Chemical Aging. *Chem. Sci.* **2016**, *7* (2), 1357–1367. https://doi.org/10.1039/c5sc02959g.

(102) Schum, S. K.; Zhang, B.; Dzepina, K.; Fialho, P.; Mazzoleni, C.; Mazzoleni, L. R. Molecular and Physical Characteristics of Aerosol at a Remote Free Troposphere Site: Implications for Atmospheric Aging. *Atmos. Chem. Phys.* **2018**, *18* (19), 14017–14036. https://doi.org/10.5194/acp-18-14017-2018.

(103) Champion, W. M.; Rothfuss, N. E.; Petters, M. D.; Grieshop, A. P. Volatility and Viscosity Are Correlated in Terpene Secondary Organic Aerosol Formed in a Flow Reactor. *Environ. Sci. Technol. Lett.* **2019**. https://doi.org/10.1021/acs.estlett.9b00412.

(104) Saukko, E.; Lambe, A. T.; Massoli, P.; Koop, T.; Wright, J. P.; Croasdale, D. R.; Pedernera, D. A.; Onasch, T. B.; Laaksonen, A.; Davidovits, P.; Worsnop, D. R.; Virtanen, A. Humidity-Dependent Phase State of SOA Particles from Biogenic and Anthropogenic Precursors. *Atmos. Chem. Phys.* **2012**, *12* (16), 7517–7529. https://doi.org/10.5194/acp-12-7517-2012.

(105) Li, Y.; Day, D. A.; Stark, H.; Jimenez, J.; Shiraiwa, M. Predictions of the Glass Transition Temperature and Viscosity of Organic Aerosols by Volatility Distributions. *Atmos. Chem. Phys.* **2020**, *20* (13), 8103–8122. https://doi.org/10.5194/acp-2019-1132.

(106) Jain, S.; Fischer, K. B.; Petrucci, G. A. The Influence of Absolute Mass Loading of Secondary Organic Aerosols on Their Phase State. *Atmosphere (Basel).* **2018**, *9* (4). https://doi.org/10.3390/atmos9040131.

(107) Champion, W. M.; Rothfuss, N. E.; Petters, M. D.; Grieshop, A. P. Volatility and Viscosity Are Correlated in Terpene Secondary Organic Aerosol Formed in a Flow Reactor. *Environ. Sci. Technol. Lett.* **2019**, *6* (9), 513–519. https://doi.org/10.1021/acs.estlett.9b00412.

(108) Tsimpidi, A. P.; Karydis, V. A.; Pandis, S. N.; Lelieveld, J. Global Combustion Sources of Organic Aerosols: Model Comparison with 84 AMS Factor-Analysis Data Sets. *Atmos. Chem. Phys.* **2016**, *16* (14), 8939–8962. https://doi.org/10.5194/acp-16-8939-2016.

(109) Guenther, A.; Jiang, X.; Shah, T.; Huang, L.; Kemball-Cook, S.; Yarwood, G. Model of Emissions of Gases and Aerosol from Nature Version 3 (MEGAN3) for Estimating Biogenic Emissions. In *Air Pollution Modeling and its Application XXVI*; Mensink, C., Gong, W., Hakami, A., Eds.; Springer International Publishing: Cham, 2020; pp 187–192.

(110) Song, M.; Liu, P. F.; Hanna, S. J.; Li, Y. J.; Martin, S. T.; Bertram, A. K. Relative Humidity-Dependent Viscosities of Isoprene-Derived Secondary Organic Material and Atmospheric Implications for Isoprene-Dominant Forests. *Atmos. Chem. Phys.* **2015**, *15* (9), 5145–5159. https://doi.org/10.5194/acp-15-5145-2015.

(111) Ditto, J. C.; Joo, T.; Khare, P.; Sheu, R.; Takeuchi, M.; Chen, Y.; Xu, W.; Bui, A. A. T.; Sun, Y.; Ng, N. L.; Gentner, D. R. Effects of Molecular-Level Compositional Variability in Organic Aerosol on Phase State and Thermodynamic Mixing Behavior. *Environ. Sci. Technol.* **2019**. https://doi.org/10.1021/acs.est.9b02664.

(112) Bateman, A. P.; Gong, Z.; Liu, P.; Sato, B.; Cirino, G.; Zhang, Y.; Artaxo, P.; Bertram, A. K.; Manzi, A. O.; Rizzo, L. V; Souza, R. A. F.; Zaveri, R. A.; Martin, S. T. Sub-Micrometre Particulate Matter Is Primarily in Liquid Form over Amazon Rainforest. *Nat. Geosci.* **2016**, *9* (1), 34–39. https://doi.org/10.1038/ngeo2599.

(113) Ye, Q.; Robinson, E. S.; Ding, X.; Ye, P.; Sullivan, R. C.; Donahue, N. M. Mixing of Secondary Organic Aerosols versus Relative Humidity. *Proc. Natl. Acad. Sci. U. S. A.* **2016**, *113* (45), 12649–12654. https://doi.org/10.1073/pnas.1604536113.

(114) Pajunoja, A.; Hu, W.; Leong, Y. J.; Taylor, N. F.; Miettinen, P.; Palm, B. B.; Mikkonen, S.; Collins, D. R.; Jimenez, J. L.; Virtanen, A. Phase State of Ambient Aerosol Linked with Water Uptake and Chemical Aging in the Southeastern US. *Atmos. Chem. Phys.* **2016**, *16* (17), 11163–11176. https://doi.org/10.5194/acp-16-11163-2016.

(115) Bateman, A. P.; Gong, Z.; Harder, T. H.; De Sá, S. S.; Wang, B.; Castillo, P.; China, S.; Liu, Y.; O'Brien, R. E.; Palm, B. B.; Shiu, H. W.; Cirino, G. G.; Thalman, R.; Adachi, K.; Lizabeth Alexander, M.; Artaxo, P.; Bertram, A. K.; Buseck, P. R.; Gilles, M. K.; Jimenez, J. L.; Laskin, A.; Manzi, A. O.; Sedlacek, A.; Souza, R. A. F.; Wang, J.; Zaveri, R.; Martin, S. T. Anthropogenic Influences on the Physical State of Submicron Particulate Matter over a Tropical Forest. *Atmos. Chem. Phys.* **2017**, *17* (3), 1759–1773. https://doi.org/10.5194/acp-17-1759-2017.

(116) Carlson, T. N. Speculations on the Movement of Polluted Air to the Arctic. *Atmos. Environ.* **1981**, *15* (8), 1473–1477. https://doi.org/10.1016/0004-6981(81)90354-1.

(117) Weinzierl, B.; Ansmann, A.; Prospero, J. M.; Althausen, D.; Benker, N.; Chouza, F.; Dollner, M.; Farrell, D.; Fomba, W. K.; Freudenthaler, V.; Gasteiger, J.; Groß, S.; Haarig, M.; Heinold, B.; Kandler, K.; Kristensen, T. B.; Mayol-Bracero, O. L.; Müller, T.; Reitebuch, O.; Sauer, D.; Schäfler, A.; Schepanski, K.; Spanu, A.; Tegen, I.; Toledano, C.; Walser, A. The Saharan Aerosol Long-Range Transport and Aerosol-Cloud-Interaction Experiment: Overview and Selected Highlights. *Bull. Am. Meteorol. Soc.* **2017**, *98* (7), 1427–1451. https://doi.org/10.1175/BAMS-D-15-00142.1.

(118) Zhao, Z.; Cao, J.; Shen, Z.; Xu, B.; Zhu, C.; Chen, L. W. A.; Su, X.; Liu, S.; Han, Y.; Wang, G.; Ho, K. Aerosol Particles at a High-Altitude Site on the Southeast Tibetan Plateau, China: Implications for Pollution Transport from South Asia. *J. Geophys. Res. Atmos.* **2013**, *118* (19), 11,360-11,375. https://doi.org/10.1002/jgrd.50599.

(119) Zelenyuk, A.; Imre, D.; Beránek, J.; Abramson, E.; Wilson, J.; Shrivastava, M. Synergy between Secondary Organic Aerosols and Long-Range Transport of Polycyclic Aromatic Hydrocarbons. *Environ. Sci. Technol.* **2012**, *46* (22), 12459–12466. https://doi.org/10.1021/es302743z.

(120) Mu, Q.; Shiraiwa, M.; Octaviani, M.; Ma, N.; Ding, A.; Su, H.; Lammel, G.; Pöschl, U.; Cheng, Y. Temperature Effect on Phase State and Reactivity Controls Atmospheric Multiphase Chemistry and Transport of PAHs. *Sci. Adv.* **2018**, *4* (3). https://doi.org/10.1126/sciadv.aap7314.

(121) Shrivastava, M.; Lou, S.; Zelenyuk, A.; Easter, R. C.; Corley, R. A.; Thrall, B. D.; Rasch, P. J.; Fast, J. D.; Simonich, S. L. M.; Shen, H.; Tao, S. Global Long-Range Transport and Lung Cancer Risk from Polycyclic Aromatic Hydrocarbons Shielded by Coatings of Organic Aerosol. *Proc. Natl. Acad. Sci. U. S. A.* **2017**, *114* (6), 1246–1251. https://doi.org/10.1073/pnas.1618475114.

(122) Friedman, C. L.; Pierce, J. R.; Selin, N. E. Assessing the Influence of Secondary Organic versus Primary Carbonaceous Aerosols on Long-Range Atmospheric Polycyclic Aromatic Hydrocarbon Transport. *Environ. Sci. Technol.* **2014**, *48* (6), 3293–3302. https://doi.org/10.1021/es405219r.

(123) Heald, C. L.; Jacob, D. J.; Turquety, S.; Hudman, R. C.; Weber, R. J.; Sullivan, A. P.; Peltier, R. E.; Atlas, E. L.; de Gouw, J. A.; Warneke, C.; Holloway, J. S.; Neuman, J. A.; Flocke, F. M.; Seinfeld, J. H. Concentrations and Sources of Organic Carbon Aerosols in the Free Troposphere over North America. *J. Geophys. Res. Atmos.* **2006**, *111* (D23S47), 1–12. https://doi.org/10.1029/2006jd007705.

(124) Holopainen, J. K.; Virjamo, V.; Ghimire, R. P.; Blande, J. D.; Julkunen-Tiitto, R.; Kivimäenpää, M. Climate Change Effects on Secondary Compounds of Forest Trees in the Northern Hemisphere . *Frontiers in Plant Science* . 2018, p

1445.

(125) Li, T.; Holst, T.; Michelsen, A.; Rinnan, R. Amplification of Plant Volatile Defence against Insect Herbivory in a Warming Arctic Tundra. *Nat. Plants* **2019**, *5* (6), 568–574. https://doi.org/10.1038/s41477-019-0439-3.

(126) Werner, C.; Fasbender, L.; Romek, K. M.; Yáñez-Serrano, A. M.; Kreuzwieser, J. Heat Waves Change Plant Carbon Allocation Among Primary and Secondary Metabolism Altering CO2 Assimilation, Respiration, and VOC Emissions . *Frontiers in Plant Science* . 2020, p 1242.

(127) Centeno, G.; Sánchez-Reyna, G.; Ancheyta, J.; Muñoz, J. A. D.; Cardona, N. Testing Various Mixing Rules for Calculation of Viscosity of Petroleum Blends. *Fuel* **2011**, *90* (12), 3561–3570. https://doi.org/10.1016/j.fuel.2011.02.028.

(128) Rovelli, G.; Song, Y.-C.; MacLean, A. M.; Topping, D. O.; Bertram, A. K.; Reid, J. P. Comparison of Approaches for Measuring and Predicting the Viscosity of Ternary Component Aerosol Particles. *Anal. Chem.* **2019**, *91* (8), 5074–5082. https://doi.org/10.1021/acs.analchem.8b05353.

(129) Song, Y. C.; Haddrell, A. E.; Bzdek, B. R.; Reid, J. P.; Bannan, T.; Topping, D. O.; Percival, C.; Cai, C. Measurements and Predictions of Binary Component Aerosol Particle Viscosity. *J. Phys. Chem. A* **2016**, *120* (41), 8123–8137. https://doi.org/10.1021/acs.jpca.6b07835.

(130) Zhang, Y.; Chen, Y.; Lei, Z.; Olson, N. E.; Riva, M.; Koss, A. R.; Zhang, Z.; Gold, A.; Jayne, J. T.; Worsnop, D. R.; Onasch, T. B.; Kroll, J. H.; Turpin, B. J.; Ault, A. P.; Surratt, J. D. Joint Impacts of Acidity and Viscosity on the Formation of Secondary Organic Aerosol from Isoprene Epoxydiols (IEPOX) in Phase Separated Particles. *ACS Earth Sp. Chem.* **2019**, *3* (12), 2646–2658. https://doi.org/10.1021/acsearthspacechem.9b00209.

(131) Riva, M.; Chen, Y.; Zhang, Y.; Lei, Z.; Olson, N. E.; Boyer, H. C.; Narayan, S.; Yee, L. D.; Green, H. S.; Cui, T.; Zhang, Z.; Baumann, K.; Fort, M.; Edgerton, E.; Budisulistiorini, S. H.; Rose, C. A.; Ribeiro, I. O.; Oliveira, R. L. E.; Dos Santos, E. O.; Machado, C. M. D.; Szopa, S.; Zhao, Y.; Alves, E. G.; De Sá, S. S.; Hu, W.; Knipping, E. M.; Shaw, S. L.; Duvoisin Junior, S.; De Souza, R. A. F.; Palm, B. B.; Jimenez, J. L.; Glasius, M.; Goldstein, A. H.; Pye, H. O. T.; Gold, A.; Turpin, B. J.; Vizuete, W.; Martin, S. T.; Thornton, J. A.; Dutcher, C. S.; Ault, A. P.; Surratt, J. D. Increasing Isoprene Epoxydiol-to-Inorganic Sulfate Aerosol Ratio Results in Extensive Conversion of Inorganic Sulfate to Organosulfur Forms: Implications for Aerosol Physicochemical Properties. *Environ. Sci. Technol.* **2019**, *53* (15), 8682–8694. https://doi.org/10.1021/acs.est.9b01019.

(132) Hornbuckle, B. K.; England, A. W. Diurnal Variation of Vertical Temperature Gradients within a Field of Maize: Implications for Satellite Microwave Radiometry. *IEEE Geosci. Remote Sens. Lett.* **2005**, *2* (1), 74–77. https://doi.org/10.1109/LGRS.2004.841370.

(133) Liu, P. F.; Zhao, C. S.; Göbel, T.; Hallbauer, E.; Nowak, A.; Ran, L.; Xu, W. Y.; Deng, Z. Z.; Ma, N.; Mildenberger, K.; Henning, S.; Stratmann, F.; Wiedensohler, A. Hygroscopic Properties of Aerosol Particles at High Relative Humidity and Their Diurnal Variations in the North China Plain. *Atmos. Chem. Phys.* **2011**, *11* (7), 3479–3494. https://doi.org/10.5194/acp-11-3479-2011.

(134) Chepfer, H.; Brogniez, H.; Noel, V. Diurnal Variations of Cloud and Relative Humidity Profiles across the Tropics. *Sci. Rep.* **2019**, *9* (1), 1–9. https://doi.org/10.1038/s41598-019-52437-6.

(135) Chung, E. S.; Sohn, B. J.; Schmetz, J.; Koenig, M. Diurnal Variation of Upper Tropospheric Humidity and Its Relations to Convectiye Activities over Tropical Africa. *Atmos. Chem. Phys.* **2007**, *7* (10), 2489–2502. https://doi.org/10.5194/acp-7-2489-2007.

(136) Foltz, G. S.; Gray, W. M. Diurnal Variation in the Troposphere's Energy Balance. *J. Atmos. Sci.* **1979**, *36*, 1450–1466. https://doi.org/https://doi.org/10.1175/1520-0469(1979)036<1450:DVITTE>2.0.CO;2.

Global Distribution of the Phase State and Mixing Times Within Secondary Organic Aerosol Particles in the Troposphere Based on Room-Temperature Viscosity Measurements

Adrian M. Maclean[1], Ying Li[2,a], Giuseppe V. Crescenzo[1], Natalie R. Smith[2], Vlassis A. Karydis[3], Alexandra P. **Tsimpidi**[3,4], Christopher L. Butenhoff[5], Celia L. Faiola[2,6], Jos Lelieveld[7,8], Sergey A. Nizkorodov[2], Manabu Shiraiwa[2], Allan K. Bertram[1*]

[1]Department of Chemistry, University of British Columbia, Vancouver, BC, V6T 1Z1, Canada
[2]Department of Chemistry, University of California Irvine, Irvine, CA 92697, USA
[3]Institute of Energy & Climate Research, IEK-8: Troposphere, Forschungszentrum Jülich GmbH, 52428 Jülich, Germany
[4]Institute for Environmental Research & Sustainable Development, National Observatory of Athens, 15236 Palea Penteli, Greece
[5]Dept. of Physics, Portland State University, Portland, Oregon, 97201, USA
[6]Department of Ecology and Evolutionary Biology, University of California Irvine, Irvine, CA, 92697, USA
[7]Atmospheric Chemistry Department, Max Planck Institute for Chemistry, 55128 Mainz, German
[8] Energy, Environment and Water Research Center, The Cyprus Institute, Nicosia 1645, Cyprus
[a] now at: Institute of Atmospheric Physics, Chinese Academy of Sciences, Beijing, 100029, China

**Correspondence to*: Allan K. Bertram (bertram@chem.ubc.ca)

S1 Viscosity measurements of Scots pine tree SOA at 59 and 74 % RH using the poke-flow technique.

Recently, Smith et al.[1] reported the viscosity of SOA generated from the photooxidation of a mixture of volatile organic compounds used to represent the emissions from healthy Scots pine trees. Viscosities were determined using the poke-flow technique at RH values < 50%. Here we add to these previous measurements by carrying out similar measurements, but at RH values of 59 and 74 %. The same procedure was used to measure the viscosity and the same conditions were used to generate the SOA. For details of SOA generation see Smith et al.[1].

The poke-flow technique has been described previously.[2–4] The SOA is collected on a hydrophobic glass slide (coated with FluorPel 800, Cytonix) using an impactor as described in Smith et al.[1] After collection, the SOA particles on the slides were 30-80 μm in diameter. The glass slide is placed in a humidity-controlled flow cell, and humidified nitrogen is flowed through the cell to condition the particles to the surrounding RH. After conditioning the particles, a needle (13561-20, Ted Pella Company) is attached to a micromanipulator and used to poke the particles, leaving the particles in a half-torus geometry. After poking, the material flows to return to the spherical cap geometry, and images are recorded as it flows. From the images, the experimental flow time, $\tau_{flow,\,exp}$, is determined, which is defined as the time it takes for the area of the hole to reduce to a

quarter of its original size. Viscosity is then determined using fluid simulations in COMSOL Multiphysics. A half-torus is generated in COMSOL using the particle and hole dimensions from the experiments. Literature values for material properties of surface tension, density, slip length and contact angle are used as inputs (see Table S2 in Smith et al.[1]). The model also uses viscosity as an input, and the particle viscosity is determined by varying the input viscosity until the area of the hole in the model reduces to a quarter of its original size for the experimental time.

The time used to condition the particles to the surrounding RH prior to poking was 1.5-24.0 h and 3.8 h, for RH values of 59 and 74 %, respectively (Table S1). To determine if this time was sufficient for near equilibrium conditions, we first calculated the diffusion coefficients of water within the particles from the measured viscosity and using the fractional Stokes-Einstein equation (eq 10 and 11 in the main text). To evaluate eq 11 we assumed R_{diff} = 0.1 nm and R_{matrix} = 0.4 nm, as discussed in the main text, where R_{diff} is the radius of water molecules, and R_{matrix} is the radius of the organic molecules in the SOA. Once the diffusion coefficients of water were calculated, we next calculated the characteristic mixing time of water within the particles using eq 9 in the main text. Based on these calculations, the characteristic mixing times of water were always shorter than the experimental conditioning times used in the experiments, indicating that near equilibrium conditions were reached (Table S1).

S2 Viscosity of Scots pine tree SOA at 75, 85, and 95% RH based on diffusion measurements

For Scots pine tree SOA, the poke flow technique was limited RH values < 75%. At higher RH values the material flowed too fast for the poke-flow measurements. To determine viscosities of Scots pine tree SOA at higher RH values (75, 85, and 95 % RH), we first measured diffusion coefficients of large fluorescent organic molecules within the Scots pine tree SOA using rectangle area fluorescence recovery after photobleaching (rFRAP). The diffusion coefficients were then converted into viscosities using the Stokes-Einstein relation (eq 8 in the main text). The Stokes-Einstein relation together with measured diffusion coefficients should give accurate values of viscosities when the radii of the diffusing molecules are larger than the radii of the organic matrix molecules,[5,6] which is the case in our experiments. The same procedure was used to generate the Scots pine tree SOA for the rFRAP measurements as described in Smith et al.[1]. The large fluorescent organic molecule used in the current study was rhodamine 6G (R6G), which has a molecular mass of 479.02 g/mol and a radius of 0.589 nanometers.[7]

The rFRAP technique is describe in detail previously[8] and has been used to measure the diffusion of fluorescent organic molecules in SOA [9] and SOA proxies.[5,6,10] For the rFRAP experiments, glass slides (Hampton Research, 12 mm circular slides) for sample collection were first prepared by submerging them in NoChromix for 24 h, then washing the slides with methanol and water and putting them in an oven overnight. Slides were then coated with the fluorescent organic dye R6G by depositing 10 µL of a 4 mM R6G solution in ethanol on the slide and spin-coating at 6100 RPM for 1 minute. SOA was then collected on the dye coated slides using an impactor as described in Smith et al.[1]. After collection, the slides containing SOA were placed into glass jars containing saturated salt solutions of either NaCl, KCl or KNO_3 to condition the sample to the RH of choice (75, 85 and 95% RH, respectively). The samples at 75% and 85% RH were conditioned for 24 h and the sample at 95% was

conditioned for 48 h. These conditioning times were more than enough to reach equilibrium between the SOA and the surround gas phase based on calculations similar to those described in Section S1. After the SOA reached equilibrium with the RH in the jar, the jar was put into a Glove Bag™ (Glas-Col). The RH in the Glove Bag was controlled using a flow of humidified nitrogen gas, and the RH was measured using a handheld hygrometer. The RH in the bag was set to the same RH as the jar. The sample was removed from the glass jar and a siliconized glass slide was placed on top (Hampton Research, 12 mm circular slides) causing the SOA particles to form thin films approximately 15-25 μm thick, determined with a confocal laser scanning microscope. The two circular glass slides were then sandwiched between two larger glass slides coated with vacuum grease along the edges (Figure S3) to ensure the RH within the sample did not change after it was removed from the glove bag. A metal spacer was included between the two sandwiched glass slides as well to ensure there was a large enough gap between the two slides for the smaller 12 mm slides (Figure S3).

The rFRAP experiments used a 543 nm helium-neon laser on a confocal laser scanning microscope to photobleach fluorescent molecules in a specified region of the thin film. Once a rectangular region of the sample was photobleached, the bleached molecules diffused out of the area and unbleached molecules diffused in causing the fluorescence in the bleached region to recover. The time dependence of the fluorescence recovery was monitored using the confocal laser scanning microscope. From the time dependent recovery, diffusion coefficients were determined.

The rFRAP experiments were performed using a Zeiss LSM510 confocal laser scanning microscope with a 10X objective, a numerical aperture of 0.3, and a pinhole setting of 80 μm. The laser power used for bleaching was adjusted to obtain a bleach depth of 20-40%. It has previously been reported that measured diffusion coefficients are independent of bleach depth up to a bleach depth of 50% for the rFRAP technique.[8] The photobleaching areas ranged from 20 μm^2 to 324 μm^2, with the smaller areas being used at lower RHs, since lower RHs resulted in lower diffusion rates. After bleaching, the sample was scanned at time intervals ranging from 5-1200 seconds. The time intervals were varied based on the rate of recovery of the fluorescence in the bleached area. Heating of the film during the photobleaching process is not expected to impact the measured diffusion coefficients. While heating may occur, thermal diffusion would be much faster than the molecular diffusion, meaning the heat would be lost to the surroundings much more rapidly than the molecules would diffuse.[10] This is consistent with previous measurements at different photobleaching sizes and powers.[9,10]

The fluorescence intensity after photobleaching can be described using the following equation:[8]

$$\frac{F(x,y,t)}{F_0(x,y)} = 1 - \frac{K_0}{4}\left[\mathrm{erf}\left(\frac{x+\frac{l_x}{2}}{\sqrt{r^2+4Dt}}\right) - \mathrm{erf}\left(\frac{x-\frac{l_x}{2}}{\sqrt{r^2+4Dt}}\right)\right] \times \left[\mathrm{erf}\left(\frac{y+\frac{l_y}{2}}{\sqrt{r^2+4Dt}}\right) - \mathrm{erf}\left(\frac{y-\frac{l_y}{2}}{\sqrt{r^2+4Dt}}\right)\right], \quad \text{(S1)}$$

where F(x,y,t) is the fluorescence intensity at position (x,y) at time t after photobleaching; $F_0(x,y)$ is the initial fluorescence intensity at position (x,y) before photobleaching; K_0 is the effective bleach depth, or the decrease in the fluorescence intensity in the photobleached area; l_y and l_x are the dimensions of the photobleached area; r is the lateral resolution of the microscope; D is the diffusion coefficient of the fluorescent molecule; and erf is the error function.

After an rFRAP experiment, the images were first normalized to an image collected before photobleaching using ImageJ.[11] The image resolution was reduced from 512x512 pixels to 128x128 pixels to reduce noise. Then each image was fit to eq S1 using a Matlab script (The Mathworks, Natick, MA, USA), with K_0 and r^2+4Dt as free parameters. The bleach width (l_x and l_y) is determined by fitting eq S1 to the first five images after photobleaching with the bleach width left as a free parameter. The value of the bleach width is then used as an input when analysing all the images. A value for r^2+4Dt is obtained from each image and is plotted as a function of time after photobleaching. The data was fit to a straight line, and the diffusion coefficient was determined from the slope of the line. An example of an r^2+4Dt plot is shown in Figure S4. Images were only used if the signal was less than 3 times the standard deviation of the noise.

Equation S1 assumes that there is no diffusion in the z direction. It has been shown that eq S1 gives accurate diffusion coefficients when the thickness of the film is ≤ 120 μm and the numerical aperture of the microscope is ≤ 0.45,[8] which is the case in our experiments.

S3 Activity based viscosity mixing rule

The activity based mixing rule is based on the Arrhenius mixing rule:

$$\log(\eta_{mix}) = x_{SOA}\log(\eta_{SOA}) + x_{H2O}\log(\eta_{H2O}), \text{ (S2)}$$

where η_{mix}, η_{SOA} and η_{H2O} are the viscosity of the mixture, SOA, and water, respectively, and x_{SOA} and x_{H2O} are the mole fraction of the SOA and water in the mixture. The mole fraction of water and SOA can be calculated from the relative humidity (RH) using the following equation:[12]

$$a_w = \frac{1}{(1+i_{\mathrm{SOA}}\frac{n_{\mathrm{SOA}}}{n_{\mathrm{H2O}}})}, \text{ (S3)}$$

where a_w is the activity of water, i is the van't Hoff factor, and n_{SOA} and n_{H2O} are the moles of water and SOA, respectively. We assumed a van't Hoff factor of 1. This allows the equation to be rearranged into the form:

$$a_w = \frac{n_{\mathrm{H2O}}}{(n_{\mathrm{H2O}}+n_{\mathrm{SOA}})}, \text{ (S4)}$$

This equation shows that the mole fraction of water is equal to the activity of water in an ideal solution with a van't Hoff factor of 1. The activity of water is defined as $\frac{RH}{100}$, which can be combine with equation S2 to give the final activity based mixing rule:

$$\log(\eta) = (1 - \frac{RH}{100})\log(\eta_{SOA}) + \frac{RH}{100}\log(\eta_{H2O}), \text{ (S5)}$$

S4 Viscosity of water as a function of temperature

The viscosity of water as a function of temperature was determined based on the temperature-dependent viscosities between 311 K and 230 K from Hallett[13] and Crittenden et al.[14] (Figure S5). The data was fit to the VTF equation:[15]

$$\log(\eta) = A + \frac{B}{(T-T_0)}, \text{ (S6)}$$

where A and B are fitting constants. The VTF equation is an empirical equation that has been used to fit temperature-dependence viscosity data for a wide variety of compounds.[15] The values of [A, B, and T_0] obtained from the fitting were [-4.28 ± 0.011, 152.87 ± 2.21, 173.06 ± 0.70]. The fit to the data is shown in Figure S5 as a solid line.

Tables and Figures

Table S1: Relevant experimental conditions used in the poke-flow experiments. RH is the relative humidity at which the experiments were carried out. The midpoint of viscosity is based on the poke-flow measurements. The diffusion coefficient of water was calculated from the viscosity and the fractional Stokes-Einstein equation. The d_p-values listed here are the diameter of the droplets used in the poke-flow experiments. These d_p-values are different than the d_p-value used when calculating mixing times in SOA in the atmosphere (see main text). For the latter we used a d_p-value of 200 nm, which corresponds to a common size of SOA particles in the atmosphere. The $\tau_{mix,H2O}$-values are the calculated characteristic mixing time of water within the particles based on the calculated diffusion coefficients of water. The $t_{exp,H2O}$-values are the experimental conditioning times, or the time allowed for the particles to come to equilibrium with the surrounding RH.

RH (%)	Midpoint of viscosity (Pa s)	Diffusion coefficient of water (m^2 s^{-1})	d_p (μm)	$\tau_{mix,H2O}$ (hrs)	$t_{exp,H2O}$ (hrs)
59	$2x10^4$	$3x10^{-13}$	55-59	0.08-0.09	1.5-24
74	$1x10^3$	$1x10^{-12}$	58-67	0.017-0.023	3.75

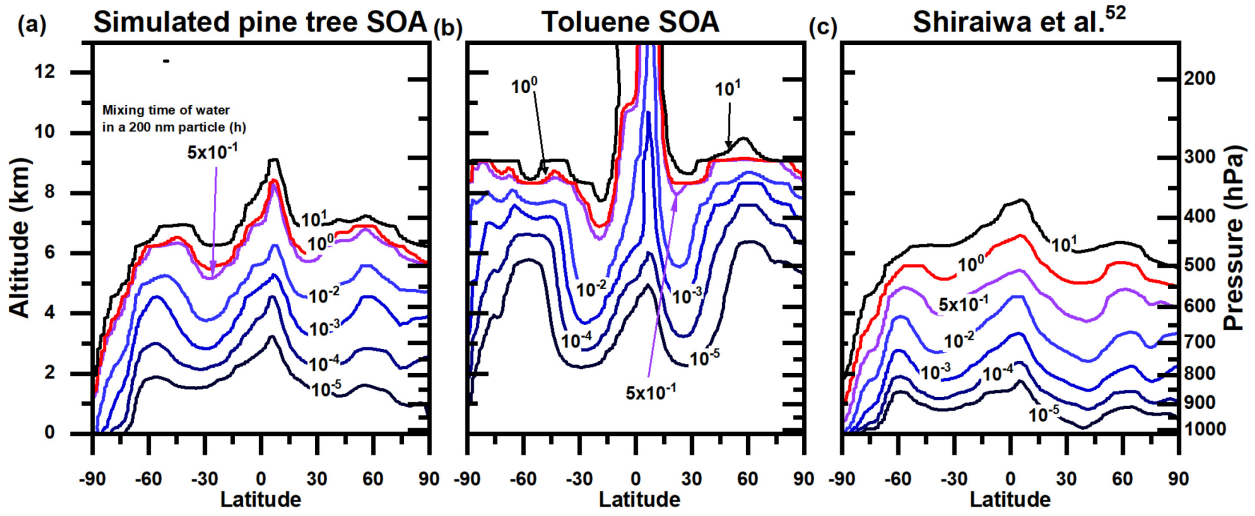

Figure S1. Annual average mixing time of water in a 200 nm particle for a) simulated pine tree SOA, b) toluene SOA, and c) SOA from Shiraiwa et al.[52] as a function of altitude and latitude. The contour lines correspond to mixing times in hours. The red contour line corresponds to a mixing time of 1 h and the purple contour line corresponds to a mixing time of 0.5 h.

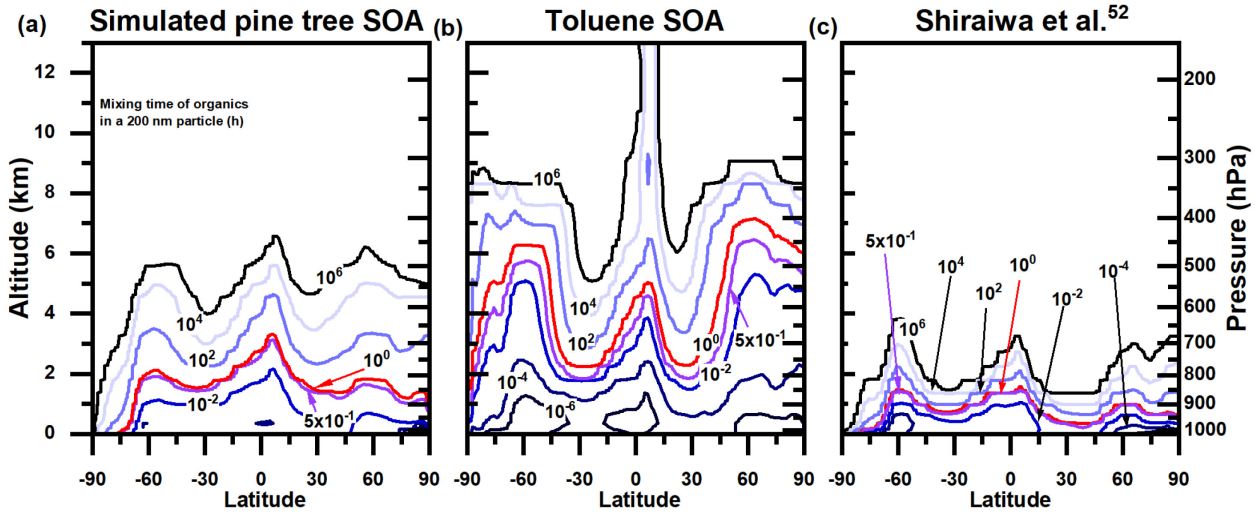

Figure S2. Annual average mixing time of organic molecules within SOA for a) simulated pine tree SOA, b) toluene SOA, and c) SOA from Shiraiwa et al.[52] as a function of altitude and latitude. The contour lines correspond to mixing times in hours. The red contour line corresponds to a mixing time of 1 h and the purple contour line corresponds to a mixing time of 0.5 h.

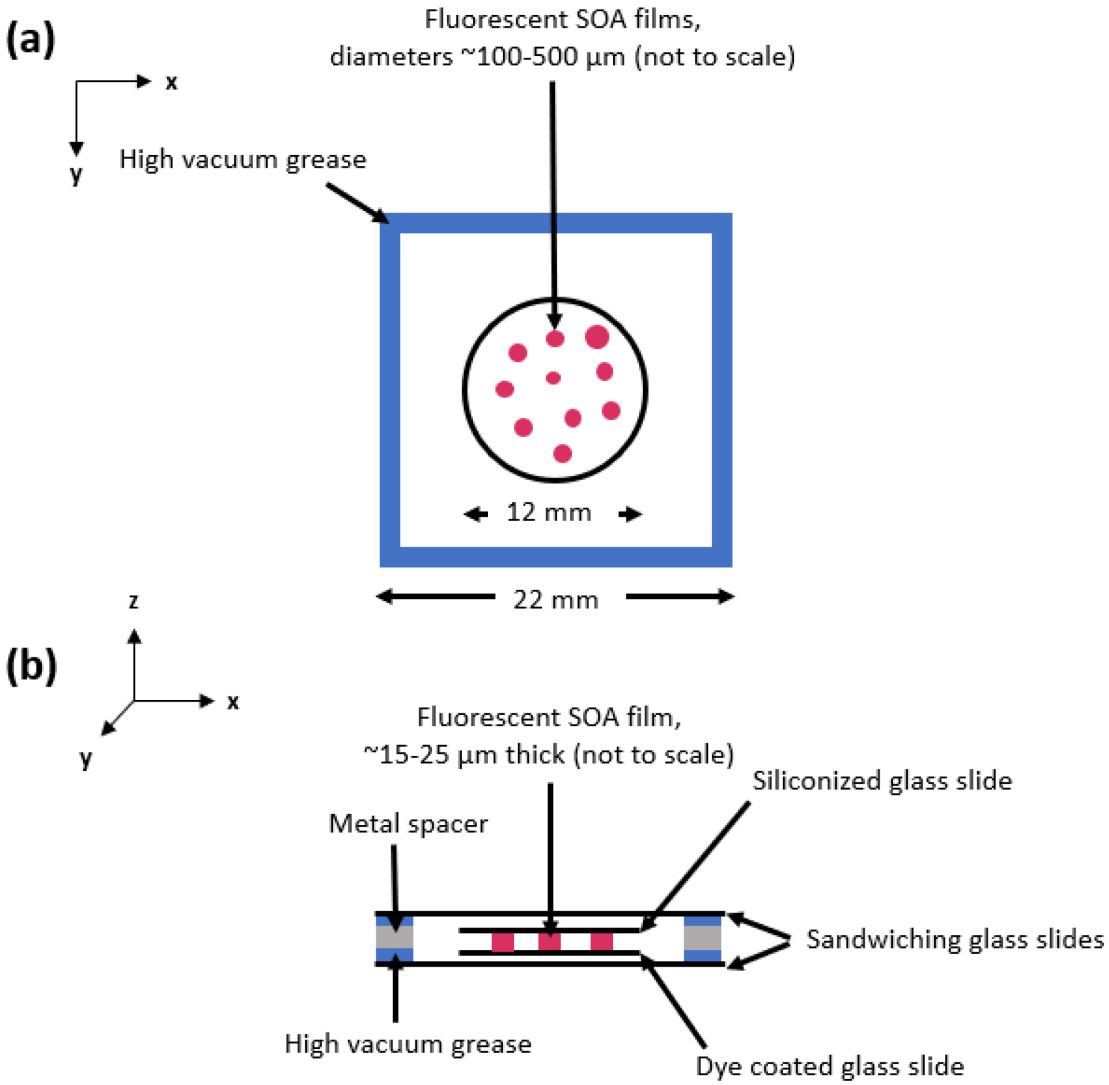

\

Figure S3. Schematic of a prepared rFRAP sample. Panel A shows a top view and panel B shows a side view of the prepared sample.

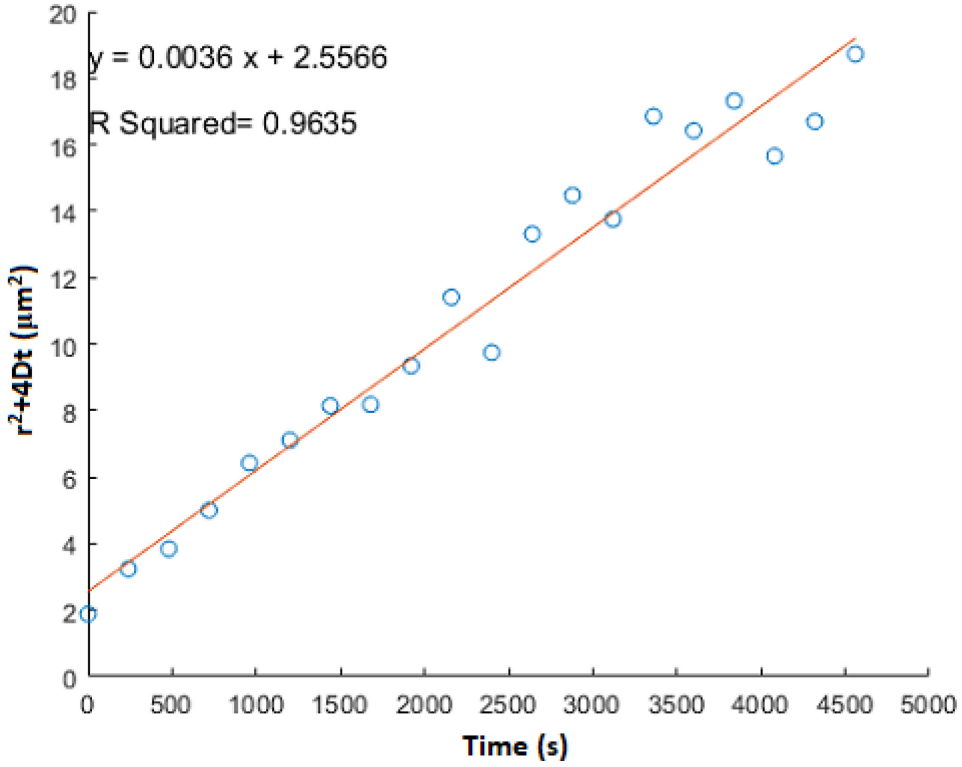

Figure S4. Plot of r^2+4Dt as a function of time after a SOA sample containing a fluorescent organic dye (Rhodamine 6G) was photobleached at an RH of 85%. Each circle corresponds to a value obtained from the fit of eq S1 to one of the images recorded after photobleaching and the red line corresponds to the linear best fit to the data.

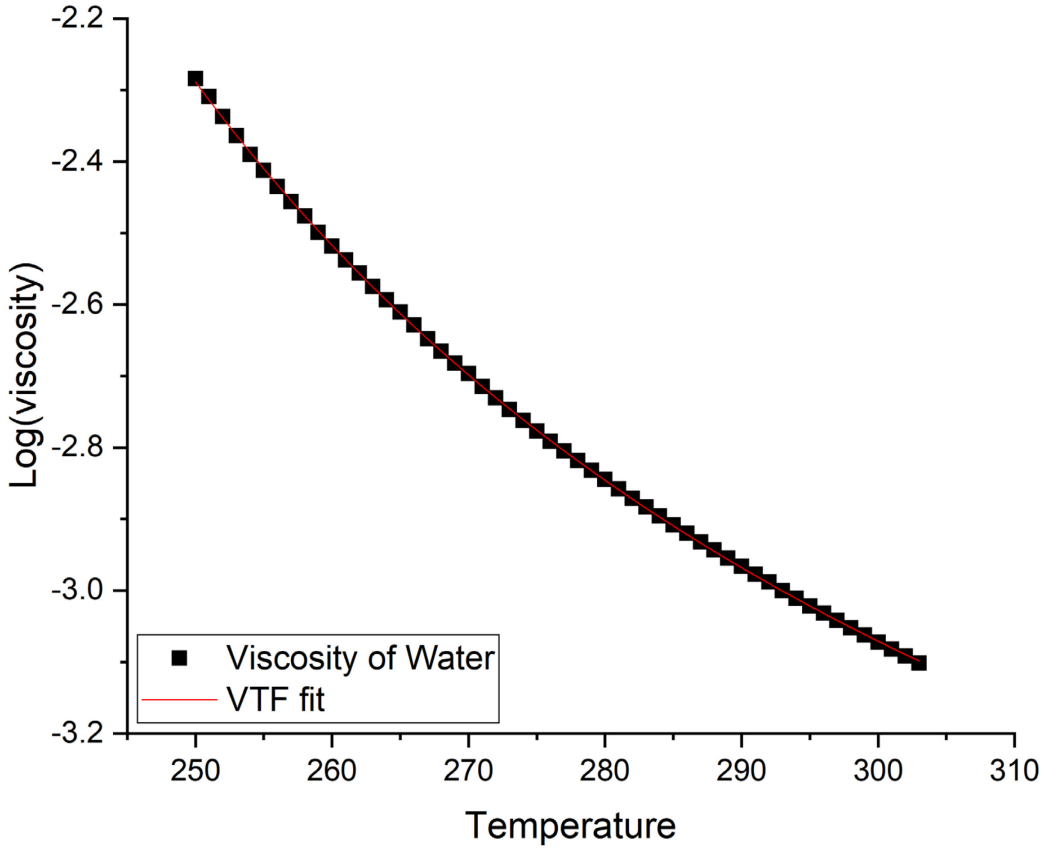

Figure S5. Viscosity as a function of temperature for water and fit to the experimental data using the VTF equation. The black squares correspond to the measured viscosities of water as a function of temperature from Hallett[13] and Crittenden et al.[14] and the red line is a fit to the data using the VTF equation (eq S6).

References

(1) Smith, N. R.; Crescenzo, G. V.; Huang, Y.; Hettiyadura, A. P. S.; Siemens, K.; Li, Y.; Faiola, C. L.; Laskin, A.; Shiraiwa, M.; Bertram, A. K.; Nizkorodov, S. A. Viscosity and Liquid–Liquid Phase Separation in Healthy and Stressed Plant SOA. *Environ. Sci. Atmos.* **2021**, *1* (3), 140–153. https://doi.org/10.1039/d0ea00020e.

(2) Grayson, J. W.; Song, M.; Sellier, M.; Bertram, A. K. Validation of the Poke-Flow Technique Combined with Simulations of Fluid Flow for Determining Viscosities in Samples with Small Volumes and High Viscosities. *Atmos. Meas. Tech.* **2015**, *8* (6), 2463–2472. https://doi.org/10.5194/amt-8-2463-2015.

(3) Grayson, J. W.; Zhang, Y.; Mutzel, A.; Renbaum-Wolff, L.; Böge, O.; Kamal, S.; Herrmann, H.; Martin, S. T.; Bertram, A. K. Effect of Varying Experimental Conditions on the Viscosity of α-Pinene Derived Secondary Organic Material. *Atmos. Chem. Phys.* **2016**, *16* (10), 6027–6040. https://doi.org/10.5194/acp-16-6027-2016.

(4) Renbaum-Wolff, L.; Grayson, J. W.; Bateman, A. P.; Kuwata, M.; Sellier, M.; Murray, B. J.; Shilling, J. E.; Martin, S. T.; Bertram, A. K. Viscosity of α-Pinene Secondary Organic Material and Implications for Particle Growth and Reactivity. *Proc. Natl. Acad. Sci. U. S. A.* **2013**, *110* (20), 8014–8019. https://doi.org/10.1073/pnas.1219548110.

(5) Evoy, E.; Kamal, S.; Patey, G. N.; Martin, S. T.; Bertram, A. K. Unified Description of Diffusion Coefficients from Small to Large Molecules in Organic-Water Mixtures. *J. Phys. Chem. A* **2020**, *124* (11), 2301–2308. https://doi.org/10.1021/acs.jpca.9b11271.

(6) Evoy, E.; Maclean, A. M.; Rovelli, G.; Li, Y.; Tsimpidi, A. P.; Karydis, V. A.; Kamal, S.; Lelieveld, J.; Shiraiwa, M.; Reid, J. P.; Bertram, A. K. Predictions of Diffusion Rates of Large Organic Molecules in Secondary Organic Aerosols Using the Stokes-Einstein and Fractional Stokes-Einstein Relations. *Atmos. Chem. Phys.* **2019**, *19* (15), 10073–10085. https://doi.org/10.5194/acp-19-10073-2019.

(7) Müller, C. B.; Loman, A.; Pacheco, V.; Koberling, F.; Willbold, D.; Richtering, W.; Enderlein, J. Precise Measurement of Diffusion by Multi-Color Dual-Focus Fluorescence Correlation Spectroscopy. *EPL* **2008**, *80* (4), 46001.

(8) Deschout, H.; Hagman, J.; Fransson, S.; Jonasson, J.; Rudemo, M.; Loren, N.; Braeckmans, K. Straightforward FRAP for Quantitative Diffusion Measurements with a Laser Scanning Microscope. *Opt. Express* **2010**, *18* (22), 22886–22905. https://doi.org/10.1364/oe.18.022886.

(9) Ullmann, D. A.; Hinks, M. L.; Maclean, A. M.; Butenhoff, C. L.; Grayson, J. W.; Barsanti, K.; Jimenez, J. L.; Nizkorodov, S. A.; Kamal, S.; Bertram, A. K. Viscosities, Diffusion Coefficients, and Mixing Times of Intrinsic Fluorescent Organic Molecules in Brown Limonene Secondary Organic Aerosol and Tests of the Stokes–Einstein Equation. *Atmos. Chem. Phys.* **2019**, *19* (3), 1491–1503. https://doi.org/10.5194/acp-19-1491-2019.

(10) Chenyakin, Y.; Ullmann, D. A.; Evoy, E.; Renbaum-Wolff, L.; Kamal, S.; Bertram, A. K. Diffusion Coefficients of Organic Molecules in Sucrose-Water Solutions and Comparison with Stokes-Einstein Predictions. *Atmos. Chem. Phys.*

2017, *17* (3), 2423–2435. https://doi.org/10.5194/acp-2016-740.

(11) Schneider, C. A.; Rasband, W. S.; Eliceiri, K. W. NIH Image to ImageJ: 25 Years of Image Analysis. *Nat. Methods* **2012**, *9* (7), 671–675. https://doi.org/10.1007/978-1-84882-087-6_9.

(12) Koop, T.; Bookhold, J.; Shiraiwa, M.; Pöschl, U. Glass Transition and Phase State of Organic Compounds: Dependency on Molecular Properties and Implications for Secondary Organic Aerosols in the Atmosphere. *Phys. Chem. Chem. Phys.* **2011**, *13* (43), 19238–19255. https://doi.org/10.1039/c1cp22617g.

(13) Hallett, J. The Temperature Dependence of the Viscosity of Supercooled Water. *Proc. Phys. Soc.* **1963**, *82* (6), 1046–1050. https://doi.org/10.1088/0370-1328/82/6/326.

(14) Crittenden, J. C.; Trussel, R. R.; Hand, D. W.; Howe, K. J.; Tchobanoglous, G. *MWH's Water Treatment*; John Wiley and Sons, 2012.

(15) Angell, C. A. Relaxation in Liquids, Polymers and Plastic Crystals - Strong/Fragile Patterns and Problems. *J. Non. Cryst. Solids* **1991**, *133*, 13–31.